COPY OF MY PHD THESIS AS AVAILABLE IN LIBRARY OF UNIVERSITY OF HOUSTON, U.S.: Gestational lead exposure shortens cell cycle length and activates developmental molecular network of neurogenesis in postnatal retina

Shradha Mukherjee

Gestational lead exposure shortens cell cycle length and activates developmental molecular network of neurogenesis in postnatal retina.

Short Running Title: Gestational lead exposure shortens cell cycle

Shradha Mukherjee[1], Shawnta Y Chaney[1], Anand Gidabbasappa[1], Elda Rueda[2], Jerry E. Johnson[3], Anand Swaroop[4], Matthew J. Brooks[4], Donald A. Fox[1,2,4]

[1]Department of Biology and Biochemistry, University of Houston, Houston, TX 77204; [2]College of Optometry, University of Houston, Houston, TX 77204; [3]University of Houston-Downtown, Houston, TX 77004; [4]Neurobiology Neurodegeneration and Repair Laboratory, National Eye Institute, NIH, Bethesda, MD 20892; [4]Department of Pharmacology and Pharmaceutical Science, University of Houston, Houston, TX 77204

Source: University of Houston (UH) PhD Biochemistry Thesis of Student Student Shradha Mukherjee, PhD Email: smukher2@yahoo.com.

Shradha Mukherjee: Email: smukher2@yahoo.com
UH Faculty PhD Advisor: *Donald A. Fox, PhD*

ABSTRACT

Background: Low level gestational lead exposure (GLE) produces increased number of rod photoreceptors and supernormal eletroretinograms (ERGs) in children and rodents. This contrasts with known apoptotic loss of rod photoreceptors and subnormal ERG of high level adult Lead exposure.

Objectives: The goal of this study was to decipher the underlying cellular and molecular mechanisms of this novel GLE phenotype in our murine GLE model. We hypothesized that cell cycle reentry of retinal progenitor cells (RPCs) and cell cycle exit, and rod photoreceptor cell fate specification of RPCs would be higher in GLE relative to control retinas and would occur with concurrent molecular changes.

Methods: Female C57BL/6 mice were exposed to lead through drinking water 2 weeks before mating, throughout gestation till postnatal day 10 (PN10). Blood lead concentrations ([BPb]) in controls and GLE pups were ≤ 1 and 25 µg/dL, respectively, at PN10. Retinas from pups aged PN2 to PN10 were used to perform retinal experiments.

Results: Cumulative BrdU labeling revealed that GLE shortens cell cycle length at G1-phase and accelerates cell cycle. Affymetrix gene expression array, qPCR, Western blot and confocal microscopy showed that GLE increases alters NOTCH1-HES1 pathway, cell cycle regulators (Cyclins, INKs, p27KIP, RB phophorylation) and bHLH (ASCL1, OTX2, HES6) rod photoreceptor differentiation regulators, without change in spatiotemporal expression pattern. In both GLE and control retinas, we found a spatial coupling of regulators of cell cycle exit (p27KIP), cell cycle inhibitors (p16, p19 INKs), cell cycle

reentry (HES1), cell fate specification (ASCL1, OTX2, HES1) in the SVZ, while cell cycle progression regulators (Cyclins) were spatially uncoupled and located in the inner retina. ChIP-qPCR showed increased activity of Cyclin D1 and ASCL1 promoters in GLE retinas.

Conclusions: Our findings show that GLE shortens cell cycle to increase proliferation and rod photoreceptor differentiation of RPCs, and this is mediated through differential expression of the NOTCH1-HES1 signaling, cell cycle regulators (Cyclins, INKs, CIP/KIP) and differentiation factors (ASCL1, OTX2). Our results suggest that there is greater cross-talk between the spatiotemporally coupled processes of cell cycle inhibition (INKS, KIP), cell fate specification factors (ASCL1, OTX2, HES1) and cell cycle reentry mediated by HES1 than with spatiotemporally uncoupled cell cycle progression regulation by Cyclins, and this spatiotemporal segregation may provide an insurance to proper transition of RPCs through these developmental stages. These results provide new insights into the molecular mechanism of retinal development and GLE effects.

Abbreviations: AC: Amacrine cell, BC: Bipolar cell, BrdU: 5-bromo-2-deoxyuridine, E: embryonic day, GCL: ganglion cell layer, GLE: gestational lead exposure, INL: inner nuclear layer, IR: immunoreactive, LSCM: laser scanning confocal microscopy, NBL: neuroblastic layer, ONL: outer nuclear layer, PH3: phosphohistone H3, PN: postnatal day, RPC: Retinal progenitor cell

Keywords: rod photoreceptors, retina, progenitor cells, gestational lead exposure, neurogenesis, cell cycle, cell fate specification, cell cycle exit.

INTRODUCTION

Although lead continues to be removed from its biggest sources in gasoline, water pipes and paint worldwide, it remains an environmental health concern, especially for children who are most susceptible to lead exposure due to greater absorption of ingested lead and greater vulnerability of their developing nervous system relative to adults (Bellinger 2008; Leggett 1993). The current Centers for Disease Control and Prevention (CDC) level of concern for lead is blood lead concentrations ([BPb]) < 10 µg/dL and there are half a million children between 1 to 5 years old, in U.S. alone with [BPb] > 5 µg/dL. Lead is a persistent and potent developmental brain, auditory and retinal neurotoxicant (Bellinger 2008; Laughlin et al. 2009; Mendola et al. 2002; Otto and Fox 1993; Rothenberg et al. 2002) whose pathophysiological effects depend on dosage, duration and age at the time of exposure. For example, lead exposure during postnatal development and at high dosage ([BPb] > 10 µg/dL) in monkeys and rodents as well as in occupationally lead-exposed workers or adult rats produces long-term rod photoreceptor-selective visual deficits, decreased rod-mediated (scotopic) electroretinograms (ERGs) and/or rod-selective apoptosis (Fox and Boyes 2013; Fox 2015). In marked contrast, gestational lead exposure (GLE) at low dosage ([BPb] < 10 µg/dL) in humans and rodents produces supernormal scotopic ERGs (Fox et al. 2008; Nagpal and Brodie 2009; Rothenberg et al. 2002), increased and prolonged proliferation of retinal progenitor cells (RPCs) (Fox et al. 2008; Giddabasappa et al. 2011) and increased differentiation but delayed maturation of late-born rods and bipolar cells without changing normal retinal programmed cell death (Chaney et al. 2016; Fox et al. 2008; Giddabasappa et al. 2011). Other studies have shown that low level lead exposure ([BPb] < 10 µg/dL) produces deficiency in intellectual ability of children (Canfield et al. 2003; Jusko et al. 2008) and increase susceptibility to late onset neurological diseases, such as Alzheimer's disease (Basha et al. 2005; Wu et al. 2008). Lead exposure produces potent and varied detrimental effects on the brain and visual system of humans and rodent models, where the exact phenotypic outcome is determined by the timing, duration and dose of lead exposure.

Several studies have been conducted to determine the underlying molecular mechanism by which lead exerts its adverse effects on the brain and visual system. High lead exposure at 0.4 to 1.9 uM Pb alters global methylation status of neuronal genes (Neurog1, Lhx3, Plxna4, Efna2 and Grik4 genes in differentiating embryonic stem cell) (Senut et al. 2014) and impairs proliferation through activation of oxidative stress NRF2 pathway at 1mM Pb in in vitro neural stem cells (Wagner et al. 2017). Lead induces rod photoreceptor selective apoptosis through calcium overload and cytochrome c-caspase cascade in rodent retinas, and neuronal apoptosis in the brain is thought to also be mediated through calcium binding enzymes (Fox et al. 1997; He et al. 2003; Sobieniecki et al. 2015). Long-term neurological deficits were found due to lead exposure blocking PKC signaling in neurologic tissue (Pokorski et al. 1999; Vazquez and Pena de Ortiz 2004). In animal models lead induced activation of ERK1/2, and p38 (MAPK) signaling (Cordova et al. 2004; Leal et al. 2006) in cerebellum of catfish and hippocampus of brain, respectively. Neuronal differentiation and maturation genes, are targeted by low lead exposure ([BPb] < 10 µg/dL) during maturation of retinal neurons (Chx10, Otx2, PKC-alpha, VGlut1 and PMCA genes in rod photoreceptor and bipolar neurons) (Chaney et al. 2016) in GLE murine model and in adult brain neurons (Ngn1, Bdnf, Grin1, Grin2D, Grik5,

Gria4, and Grm6 genes in hippocampal neurons and embryonic stem cell derived neurons) (Sanchez-Martin et al. 2013). Initial studies to determine if cell cycle progression and differentiation of RPCs was altered in low lead exposure ([BPb] < 10 µg/dL) in retinas showed increased incorporation of M-phase and S-phase markers, PH3 and BrdU in RPCs and increased number of differentiated neurons (rod photoreceptors and bipolar cells) from GLE mice (Giddabasappa et al. 2011). However, a quantitative measurement of the individual phases of the cell cycle and cell fate specification, and the molecular mechanism underlying this novel phenotype of increased RPC proliferation and neuronal differentiation by GLE was not determined. Retina and brain are both parts of the central nervous system. Thus, assessing the molecular mechanisms of how GLE effects RPC proliferation and differentiation will be advantageous to gain generalized insights and counter the detrimental effects of lead exposure on the developing central nervous system of children.

In the developing mouse retina, six neuronal cell types and the Müller glial cell are generated from a common pool of multipotent RPCs during a two-week period beginning on embryonic day 11(Cepko 2014). During retinal development, the RPCs proliferate and differentiate into different cell types in a fixed histogenic order such that retinal ganglion cells, cone photoreceptors, horizontal cells and most amacrine cells are born prior to birth (early-born cells) and then rods, bipolar cells and the Müller glial cell are born postnatally (late-born cells) (Cepko 2014; Marquardt and Gruss 2002; Young 1985b). Together, the late-born rods (70%), bipolar cells (7-8%) and Müller glial cells (2-3%) comprise ~80% of the total number of retinal cells(Jeon et al. 1998; Rapaport et al. 2004). During cell cycle progression, the RPCs undergo interkinetic movement, during which S-phase RPC cell bodies move from the inner retina or inner neuroblast layer (INBL) to the outer retina or outer neuroblast layer (ONBL) for M-phase RPC cell bodies, while G1-phase and G2-phase RPC cell bodies remain in between these layers (Baye and Link 2008). At the time of mitosis, RPCs can divide in a symmetric or asymmetric manner and redistribute the cell intrinsic factors, allowing for daughter RPCs to take similar or different developmental paths of cell cycle reentry or cell cycle exit followed by differentiation (Baye and Link 2007).As most of the differentiated cells (neurons and glial cells) are gradually generated postnatally from the proliferating RPCs whose cell cycle phase specific location is known, postnatal RPCs are a great system to study the cellular dynamics and molecular regulation of the competing processes of cell cycle progression, cell cycle exit and neuronal-glial cell fate specification or differentiation of RPCs in a cell cycle phase specific manner.

The essential molecular switch for cell cycle entry and progression is phosphorylation of Retinoblastoma (RB), and other protein by a family of cyclin dependent kinases (CDKs), CDK 2, 4, 6. Phosphorylated RB releases the transcription factor E2F from the RB complex and is required for transcription of E2F cell cycle target genes. Regulation of cell cycle is achieved by activation and inhibition of CDK kinase activity (Sherr and Roberts 1999). These key regulators of CDKs are cyclins (Cyclins D, E, A and B) that activate kinase activity of CDKs upon binding, while CDKs are inhibited by binding of cyclin dependent kinase inhibitors (CDKIs) of the Ink4 family (p15INK4b, p16INK4a, p18INKc and p19INK4d) and the Kip family (p21CIP1, p27KIP1 and p57KIP2) (Malumbres and Barbacid 2001). This dual CDK activity regulatory mechanism ensures tight control of initiation, progression, termination and length of cell cycle, and its phases.

Increased activity of CDKs shortens cell cycle length and promotes cell cycle progression, while decreased activity of CDKs lengthens cell cycle length and promotes cell cycle exit (Alexiades and Cepko 1996; Livesey and Cepko 2001). During terminal cell cycle exit for RPC differentiation, Kips family show additional specialization and 90% of the RPCs utilize and upregulate p27KIP1 postnatally and p57KIP2 prenatally (Dyer and Cepko 2001).

Upon exit from cell cycle RPCs choose wither a neuronal or glial cell fate. This choice is tightly regulated by neuronal basis-helix-loop-helix (bHLH) and homeodomain (HD) transcription factors, NOTCH1-Hes1 pathway and JAK/STAT pathway, which results in activation one cell fate choice and inhibition of other choices, to ensure correct ratio of neuronal and glial cell in the retina. The combination of bHLH transcription factors ASCL1 (MASH1), NEUROD1 and OTX2 HD transcription factor, actively promote rod photoreceptor and bipolar cell neuronal cell fate genes, while inhibiting Muller glial cell fate in RPCs (Ahmad et al. 1998; Hatakeyama and Kageyama 2004). Proneuronal bHLH transcription factors, such as MASH1 block glial cell fate of RPCs by inducing expression of HES6, which forms inactive protein heterodimers with HES1 that blocks the ability of HES1 to transcribe its target genes (Bae et al. 2000; Gratton et al. 2003). MASH1, NGN1 and other proneural transcriptional factors can directly inhibit the gliogenic JAK/STAT pathway and by sequestering the SMADs, which are coactivators of STAT3 and thereby block the ability of STAT3 to activate its target genes (Sun et al. 2001; Vetter and Moore 2001). On the other hand, the combination of NOTCH1-DELTA pathway induced bHLH transcription factor HES1 (Furukawa et al. 2000; Tomita et al. 1996) and CNTF/LIF mediated JAK pathway induced STAT3 phosphorylation (Goureau et al. 2004; Rhee and Yang 2010), actively promotes expression of genes necessary for RPCs to take a Muller glial cell fate, while inhibiting a neuronal cell fate. Proglial transcriptional factors, HES1 and STAT3 directly inhibit proneuronal factors by HES1 mediated sequestering of MASH1 and proneuronal bHLH factor coactivator E47 (Sasai et al. 1992) and STAT3 mediated transcription of ID1/4 genes, which form inactive heterodimers MASH1 and other proneuronal factors, thus preventing induction of neuronal cell fate gene expression (Fukuda and Taga 2005). Thus, the balance of cell cycle Cyclins and Inks/CDKIs dictate the cell cycle state of RPCs, while the balance of proneuronal transcription factors (bHLH and HD) and proglial transcription factors (HES1 and STAT3) dictate the cell fate specification choice of RPCs.

The stages of cell cycle reentry, cell cycle progression, cell cycle exit and cell fate specification are thought to be coupled processes such that when RPCs transition through these stages, the preceding step is required to be stalled before the next step ensues. At the molecular level this translates to the prerequisite that the molecular regulators of the preceding step are completely extinguished before upregulation of the regulators of the next step. This is supported by the observation that during postnatal retinal development expression cyclins are progressively downregulated (Barton and Levine 2008), while expression of proneuronal differentiation factors MASH1 (Nelson et al. 2009) and OTX2 (Koike et al. 2007) are upregulated. However, this distinct coupling of developmental stages does not appear to be rigid and ectopic expression of stage specific molecular regulators of can occur during transition of RPCs, allowing for a unique opportunity of cross-talk and coordination between these stages. For example, ASCL1, a regulator of neuronal cell fate specification expected to be upregulated after cell cycle exit

of RPCs, can be expressed in RPCs still in cell cycle (Brzezinski et al. 2011), while the cell cycle regulator, RB positively promotes rod photoreceptor differentiation in the postnatal retina (Zhang et al. 2004). In another intriguing example, NOTCH1-HES1 pathway which promotes glial cell fate specification of RPCs, promotes maintenance of stem cells and proliferation of RPCs, while continuing to inhibit neuronal cell fate specification (Jadhav et al. 2006a; Jadhav et al. 2006b; James et al. 2004). A common feature of the developmental process cell cycle (cyclins, INKS), cell cycle exit (p27 KIP, p57CIP) and cell fate specification (ASCL1, NEUROD1, HES1, HES6, STAT3) regulators is that their expression levels can undergo quick turnover by coordinated induction of their mRNA expression, protein phosphorylation and protein degradation (Freire et al. 2012; Shimojo et al. 2008). It may be hypothesized that when the kinetics of turnover of the regulators is shorter than the length of the developmental process they are strictly expressed in a stage specific manner in RPCs, while longer turnover kinetics than the length of the developmental process causes leakiness or ectopic expression of these regulators in preceding and following developmental stages of RPCs opening greater opportunity for cross-talk between the stages. A comprehensive study of the spatio-temporal expression (mRNA and protein) of these regulators and measurement of cell cycle dynamics is missing in the field and is required to gain insight into the extend of coordination of cell cycle, cell cycle exit and cell fate specification regulators during retinal development. Another layer of regulation and coordinated regulation arises from specialization of the different family members of cell cycle and cell fate specification regulators. Loss of Cyclin D1 decreases RPC cell cycle reentry and induced expression of Cyclin E, but not Cyclin D2 rescues the phenotype (Das et al. 2009), while another study showed specialized cis-regulatory feedback loops between rod photoreceptor and bipolar neuronal cell fate specification transcription factors fine tune neuronal subtype choice (Wang et al. 2014). Similar experiments of multigene loss of function and rescue studies or other methods of multigene expression perturbation is required to gain functional insight into cross-talk and synergy relationships, between other molecular regulators of RPC transition through cell cycle, cell cycle exit and cell fate specification.

In this study, we sought to identify the molecular regulators and changes in cell cycle dynamics involved in the novel GLE phenotype of increased RPC proliferation and rod photoreceptor, and bipolar cell differentiation, and gain a better understanding of retinal development process. Affymetrix gene expression array identified the specific molecular changes associated with GLE induced increased proliferation and rod photoreceptor, and bipolar cell differentiation. Cell cycle analysis showed that relative to control retinas, GLE shortened G1-phase of cell cycle and increased the output of cell cycle reentry, cell cycle exit and neuronal cell fate specification of RPCs, without any change in glial cell fate. We measured cell cycle dynamics and determined spatiotemporal expression pattern of this comprehensive list of GLE dependent and developmentally important cell cycle (Cyclins, p16 p19 INKs), cell cycle exit (p27 KIP), and neuronal glial cell fate specification factors (ASCL1, OTX2, HES1) in control and GLE retinas. We found that cell cycle inhibitors (p16, p19 INKs, p27KIP) and cell fate specification factors (ASCL1, OTX2, HES1) appear together in the SVZ and disappear in the inner retina, while cell cycle activators and regulators of cell cycle progression (Cyclins) shows the reverse pattern. This suggests that cell cycle exit, HES1 mediated cell cycle reentry and cell fate specification show a stronger spatial coupling, while cell cycle progression is specially uncoupled, which may

be necessary to ensure these processes can occur smoothly. Our results reveal an intricate network of developmental regulators under GLE regulation and show the relative coordinated spatiotemporal pattern of appearance and disappearance of developmental regulators in relation to cell cycle dynamics. This study increases our understanding of the molecular regulation of developing nervous system and GLE effects on it, and will help meet the challenges of detrimental effects of GLE on the developing nervous system and other developmental disorders.

METHODS

Code availability. This work does not contain any codes.

Animal model. All experimental and animal care procedures complied with the National Institutes of Health (NIH) Public Health Service Policy on the Humane Care and Use of Laboratory Animals (NIH 2002), and were approved by the Institutional Animal Care and Use Committee of the University of Houston. All animals were treated humanely and with regard for alleviation of pain and suffering. In rodents, brain and retinal development during the first postnatal week is equivalent to the last trimester of human gestation (Dobbing and Sands 1979; Martins and Pearson 2008). The murine GLE model (Fig. 1a) used has been previously described (Chaney et al. 2016; Giddabasappa et al. 2011). Briefly, naive C57BL/6 wild-type female mice were given tap water for drinking containing 0 ppm lead (Control group) or 55 ppm lead acetate (GLE group) for two weeks prior to mating, during mating and pregnancy, and until PN10, after which both groups were given lead free tap water. This treatment regimen ensured a steady lead level in the GLE pups, with peak [BPb] on PN0 and/or PN10 of 22.11 ± 1.05 µg/dL, while control group remained at [BPb] 0.75 ± 0.06 µg/dL(Leasure et al. 2008). There were no statistical differences between control and GLE groups on litter measure or body weight (Leasure et al. 2008).

Tissue processing, immunohistochemistry and confocal microscopy. All tissue processing, immunohistochemistry and confocal technique was performed essentially as described (Chaney et al. 2016; Giddabasappa et al. 2011). Briefly, eyes were removed and immersion fixed in 4% paraformaldehyde for 30min. Central retina 10um sections were cut from cryoprotected frozen retinas at 200-400um distance from optic nerve for confocal microscopy and slide mounted. Nuclear dyes and primary antibodies against retinal development regulators were used at concentrations as listed in Supplement Table 1. Mounted sections were post-fixed with 4% paraformaldehyde for 15min and treated with 1% sodium-borohydride to reduce auto-fluorescence. The sections were washed in PBS, blocked with blocking buffer (10% normal goat serum and 0.3% Triton-X100) and incubated for 48 hours at 4ºC in primary antibody solution prepared in blocking buffer. After PBS washes Alexa fluorescent, secondary antibodies (1:400) made in blocking buffer were applied to the slides for 1hour at room temperature in the dark. The sections were washed, treated with DRAQ5 and coverslipped using Vectashield Mounting Medium (Vector Laboratories Inc., Burlinghame, CA). Confocal images were taken using identical exposure and scanning parameters with a Leica TCS

SP2 LSCM (Leica Microsystems, Exton, PA). NIH ImageJ software was used to count colabeled cells at 63X magnification using the “analyze particles” protocol as previously described with a minimal particle size of 30 pixels. Mean ± SEM values from these counts were used on the images and/or used on the graphs.

In vivo cell cycle dynamics measurements: To assay cell cycle reentry and exit, cell fate specification, proliferation index and mitotic fraction we adapted for the retina previously described protocols of BrdU injection, immunohistochemistry and confocal microscopy (Chenn and Walsh 2002; Hodge et al. 2004; Young 1985a). Briefly, one dose of BrdU (100 µg/gm body weight) was intraperitoneally (ip) administered into pups. In pups sacrificed 24 hours post-BrdU injection, fraction of MCM6+BrdU+ cells, MCM6-BrdU+ cells and OTX2+BrdU+ cells relative to total BrdU+ cells were computed using confocal microscopy to determine cell cycle reentry, cell cycle exit and cell fate specification indices, respectively. In pups sacrificed 45min post-BrdU injection, RPC proliferation index at PN1 was calculated as the fraction of MCM6+BrdU+ cells relative to total MCM6+ cells.

To assay cell cycle length, we essentially adapted for the retina previously published protocols (Hodge et al. 2004; Nowakowski et al. 1989). PN1 pups were injected with BrdU (100 µg/gm body weight) intraperitoneally (ip), and sacrificed 2.5, 3.5 and 4.5 hours following the injection. From confocal images the G2+M phase length was determined as the time required to colabel all PH3+ cells with BrdU+ such that the mean ± SEM mitotic fraction equaled 1.0 ± 0.5. To determine the total cell cycle length (TC) and total S phase length (TS) BrdU (100 µg/gm body weight) was injected intraperitoneally (ip) into PN1 pups every 4 hours for 24 hours, and sacrificed 45 minutes following the last injection. From confocal images a labeling index (LI) was calculated as the proportion of Draq5+ cells that were BrdU+ at each sacrifice time. The mean ± SEM LI vs post-injection survival time was plotted for control and GLE retinas and the best-fit line for each was determined. The maximum LI value attained was the GF, while TC and TS were determined using the following equations: 1) y-intercept = GF X TS/TC, 2) time taken to reach maximum LI = TC - TS and 3) slope = 1/Tc. At the LI curve inflexion time and plateau, GF values were determined as the proportion of MCM6+, Draq5+ of total Draq5+ cells.

Affymetrix gene expression array and heat map. Expression profiling experiments were performed at the Microarray Core Facility at Kellogg Eye Center, University of Michigan. Affymetrix gene expression array was performed following protocol provided by Affymetrix, Inc. (Santa Clara,CA) and as described before (Rueda et al. 2016; Zacks et al. 2006). Total RNA was isolated with Trizol and 2 to 5ug of total RNA was used as starting material for generation of biotinylated-cRNA (complementary RNA) with Affymetrix target labeling kit. The biotinylated-cRNA was hybridized to GeneChip Mouse Genome 430 2.0 array and scanned on Affymetrix Gene Chip Scanner 3000 7G. Robust Multichip Average (RMA) algorithm was used to obtain background corrected, quantile normalized, log2 transformed expression values. Differentially expressed genes with a with mean expression values in log2 scale ≥5 in one of the conditions and fold-change between GLE and control ≥2, and p value was <0.05 were selected as GLE target genes. From the list of GLE targets, genes that classified into NIH-DAVID Gene

Ontology (GO) categories of “cell cycle” and “cell differentiation” were selected as candidate genes for further analysis. Heat map visualization of these select candidate GLE target genes was done using online tool http://www.chibi.ubc.ca/matrix2png/.

RNA Isolation and qPCR. Total RNA was extracted from retinas with Trizol reagent (Invitrogen-Gibco) and cDNA was synthesized from 1ug of total RNA using oligo dT, and random hexamers with iScript cDNA synthesis kit (Bio-Rad Cat. No. 170-8891). Intron spanning primers designed with default settings on Roche Universal Probe Library Design Center. List of primers are presented in Supplement Table 2. qPCR was performed on the cDNA with SYBR green master mix buffer (Bio-rad) and 300 nM of each forward, and reverse primers in a total volume of 25ul on Bio-Rad iCylcer platform (Bio-Rad Laboratories, Hercules, CA). After a denaturation step of 3 min at 95°C, two-step amplification conditions were 40 cycles of 30 s at 95°C and 30 s at 60°C. Relative gene mRNA expression was calculated by using the comparative threshold cycle ($\Delta\Delta$Ct) method with β-Actin as the internal normalization control. Gene expression in GLE relative to control or fold change was computed using $2\Delta\Delta$Ct.

Western Blotting. Whole cell protein was extracted from retinas with homogenization in lysis buffer (100 mM NaCl, 1 mM EGTA, 1 mM EDTA, 1 mM DTT, 1 mM PMSF, 1 mM Na3VO4, 0.25% NP-40, 30 mM NaF, 60 mM β-glycerophosphate, 20 mM sodium pyrophosphate, 1 protease inhibitor tablet, Roche Diagnostics, 10 mM Tris pH7.4). Around 20-25 µg of total protein was loaded on 8% SDS-polyacrylamide gel and transferred onto PVDF membrane. Blots were washed, blocked in blocking buffer (5% milk in TBS-T) and probed with phospho and non-phospho antibodies prepared in blocking buffer overnight at 4ºC. Antibody concentrations are listed in Supplement Table 1. GAPDH was used as the loading control for all gels. Membranes were washed and probed with HRP-conjugated secondary antibodies (1:10,000dilution) prepared in blocking buffer and imaged with chemiluminescence (ECL Plus: Amersham Biosciences, Piscataway NJ). Non-saturated blots were scanned at high-resolution (600 dpi) for densitometry analysis using Adobe Photoshop CS.

ChIP -qPCR. Retinas were cross-linked with 1% formaldehyde for 15 min at room temperature and cross-linking was quenched by adding 125mM glycine. Retinas were homogenized in cold whole cell lysis buffer containing 0.5% NP-40 for 15 min at 4ºC. Cell debris was removed and nuclei collected by centrifugation at 13,000 rpm for 10 min. Nuclear pellet was resuspended in 1% SDS sonication buffer. Chromatin was sonicated at 4ºC using Fisher Scientific Sonic Dismembrator Model 500, for 10 sec x 4 times at 10% power. Sonicated samples were immunoprecipitation (IP) with 1ug antibody conjugated Dynabeads Protein A (Invitrogen) overnight at 4ºC. A list of antibodies used is provided in Supplement Table 1. Immunoprecipitated DNA was eluted from antibody-bead complex after washing. Eluted ChIP DNA and Input DNA were reverse cross-linked overnight at 65ºC with 192 mM NaCl and treated with Protease K at room temperature for 1 hour . DNA was purified using phenol–chloroform–isoamylalcohol extraction and was analyzed by qPCR (described above) with primers spanning the promoter regions of CyclinD1 and Mash1 (Supplement Table 2). ΔCt values were obtained from four replicates normalized against the Ct value of the

input DNA. The % Input for each ChIP fraction for the TFs were calculated as % Input = 2 (-ΔCt [normalized ChIP]) × 100.

Statistical Analysis. For all confocal experiments four to five retinas were used, each from a different mouse litter at each age (PN 2, 4, 6 and 10) for control and GLE. Retinas from five to seven littermate pups were pooled per sample for each time point per treatment group for Affymetrix, qPCR, Western blot and ChIP-qPCR experiments. Data were analyzed by using ANOVA followed by post hoc multiple comparisons using Fisher's Least Significant Difference Test or the Student's T-test when only two means were compared. For all experiments, P-value lower than 0.05 was considered significant (*P<0.05). Significant differences between GLE and control are indicated with an * asterix in figures. Graphs were generated with KaleidaGraph 4.0 (Synergy Software, Reading PA). Data are represented using mean ± SEM.

RESULTS

Time dependent and GLE dependent changes in number of RPCs reentering cell cycle and exiting cell cycle with neuronal cell fate.

We wanted to determine the cell cycle and differentiation dynamics of RPCs during RPC development. Previously, we reported the GLE retinal phenotype of increased RPC proliferation, without any change in apoptosis, which resulted in an adult retina with more late-born rod and bipolar neuronal cells and no leftover RPCs (Giddabasappa et al. 2011). We hypothesized that GLE either simultaneously or sequentially increases both cell cycle reentry and neuronal cell fate specification during postnatal development. To test this hypothesis, we scored the number of RPCs reentering cell cycle (BrdU+MCM6+), exiting cell cycle (BrdU+MCM6-) and undergoing cell fate specification (BrdU+OTX2+), by staining sections 24 hours after a single BrdU pulse of BrdU (Fig. 1; Supp. Fig. 1). We found that At PN2 and PN4, 41.5 ± 5.4% and 65.3 ± 15.7% more RPCs reentered cell cycle (BrdU+MCM6+), respectively (Fig. 1b,d; Supp. Fig. 1a). RPCs exiting cell cycle (BrdU+MCM6-) from PN2 to PN6 increased by 38.0 ± 3.5% at PN2, 53.9 ± 15.1% at PN4 and 161.9 ± 16.0% at PN6 (Fig. 1b,e; Supp. Fig. 1a), an increase accompanied by a 40-50% increase in RPCs undergoing cell fate specification into rod-bipolar neurons (BrdU+OTX2+) (Fig. 1g,i; Supp. Fig. 1b). In both GLE and control retinas, the proportion of RPCs reentering cell cycle decreased with age (Fig. 1b,f; Supp. Fig. 1a), while the proportion of RPCs exiting cell cycle and undergoing cell fate specification increased with age (Fig. 1b,f,g,j; Supp. Fig. 1a,b). There was no difference in these ratios between GLE and controls.

The pattern of cell cycle reentry and cell cycle exit of RPCs in control is consistent with previous studies (Young 1985a, b), and additionally we show that the cell cycle exit pattern overlaps with rod photoreceptor and bipolar cell fate specification. In GLE we find simultaneous increases in number of RPCs undergoing cell cycle reentry, cell cycle exit and cell fate specification to rod photoreceptors, and bipolar neurons. However, GLE does not change the ratio of RPCs undergoing cell cycle, cell cycle exit and cell fate specification, which suggests that GLE does not effect the histogenic order of normal retinal development.

GLE accelerates cell cycle progression of RPCs by shortening length of G1-phase of cell cycle.

To determine the effect of GLE on cell cycle kinetics further, we measured total cell cycle length and length of cell cycle phases. For a quick assessment of cell cycle length change, we labeled PN1 RPCs with a single 45min pulse of BrdU and found GLE increases proliferation index or proportion of MCM6+BrdU+ (Supp. Fig. 1c, control 29 ± 7%, GLE 48 ± 9%). This shows that GLE shortens cell cycle, so we specifically measured the length of different phases of cell cycle to determine the exact phase or phases that were shortened by GLE. PN1 control and GLE retinas were injected with a single pulse of BrdU and sacrificed at different times, and BrdU colabeling with PH3+ mitotic marker was scored. The results showed that the combined length of the G2+M phases of cell cycle was invariant at T_{G2+M} 4.5 hours in both GLE and control retinas (Supp. Fig. 1d). To determine the total cell cycle length and length of other phases of cell cycle we utilized cumulative BrdU-labeling. Plots of the LI vs survival time for both control and GLE illustrated that labeling index (LI) increases linearly to a maximum value and then levels off (Fig. 1k). The relationship between LI and survival time was used to calculate the cell cycle length parameters. In GLE relative to control, the calculated value of Tc was shorter by 7.6 hours or 24% (31.9 ± 3.7 hours in control, 24.3 ± 0.9 hours in GLE), but Ts (11.4 ± 3.6 hours in control, 11.6 ± 2.5 hours in GLE) and GF (0.57 ± 0.02 in control, 0.57 ± 0.03 in GLE) were not different (Fig. 1k). The composite results from the cell cycle length experiments and G2+M phase analysis enable the determination of T_{G1} [G1 = Tc – Ts – (G2+M)]. In GLE retinas relative to control, the T_{G1} was 7.8 hours shorter or almost 50% less accounting for the overall decrease in cell cycle length (16.0 ± 1.9 hours in control, 8.2 ± 0.4 hours in GLE).

The control retina cell phase lengths are consistent with previously published results, Tc 31.9 ± 3.7 hours, T_{G1} 16.0 ± 1.9 hours, Ts 11.4 ± 3.6 hours and T_{G2+M} 4.5 hours (Young 1985a). Only, T_{G1} was shorter in GLE by 7.8 hours. Taken together the analysis of cell cycle dynamics in GLE shows that GLE accelerated cell cycle and increase the number of RPCs reentering cell cycle, and exiting cell cycle with neuronal cell fate specification.

GLE regulates cell cycle and neuronal differentiation gene network.

This GLE effect contrasts with normal development, during which shortening of cell cycle length increases number of RPCs reentering cell cycle at the expense of RPCs exiting cell cycle and differentiating (Julian et al. 2016; Miles and Tropepe 2016). Therefore, we endeavored to understand the molecular mechanism of this unique GLE phenotype whereby GLE shortened cell cycle, increased cell cycle reentry and yet increased cell cycle exit and differentiation. Therefore, we performed Affymetrix gene expression array in GLE and control retinas during postnatal development. We selected the postnatal development period because GLE accelerated cell cycle and increased rod-bipolar cell fate specification postnatally. A total of 822 genes were differentially expressed between GLE and control retinas (Fig. 2a). To begin to understand the biological function of these genes we performed NIH DAVID Gene Ontology (GO) analysis, which revealed “sensory perception of light stimulus”, “nervous system development”, “cell cycle” and “neuronal differentiation” as major GOs (Fig. 2a). As GLE increased cell cycle and neuronal cell fate specification for further validation and

analysis we focused on the genes in the “cell cycle” (includes cell cycle exit gene p27 Cdkn1b) and “neuronal differentiation” GOs (Fig. 2b). The differential expression of these genes in GLE supported their functional and physiological relevance. We predicted that this comprehensive study of the spatiotemporal expression of these candidate regulators of cell cycle progression, cell cycle exit and cell fate specification, and the cell cycle dynamics measurements made in this study will reveal new insights into the coupling and uncoupling of these processes in RPCs during normal development.

We used qPCR to examine the expression of these GLE target candidate genes, cell cycle/cell cycle exit genes (*CyclinD1, CyclinE2, CyclinA2, Mcm6, Cdk2, Cdk4, Rb, p107, E2f1, Notch1, Hes1, p27 Cdkn1b, p16 Cdkn2a* and *p19 Cdkn2d*) and neuronal differentiation genes (*Hes6, Mash1, Otx2* and *Neurod1*). In the cell cycle group, the temporal pattern of gene expression of cyclins (*CyclinD1, CyclinE2* and *CyclinA2*), cell proliferation marker (*Mcm6*), cell cycle kinases (*Cdk2, Cdk4*) and Notch pathway transcription factors (*Hes1, Hes6*) decreased with age consistent with completion of developmental cell cycle and were significantly upregulated in GLE relative to control by 39% or more (Fig. 2c,d,e,f,g,h,i,j). Cell cycle inhibitors (p16 Cdkn2a, p19 Cdkn2d) showed a temporal expression pattern similar to cyclins, but were significantly downregulated in GLE by 24% (Fig. 2k,l). In the cell cycle exit and differentiation gene group, expression of cell cycle exit factor *p27 Cdkn1b*, cell cycle inhibitor and rod differentiation factor *Rb1,* rod photoreceptor and bipolar neuronal differentiation factors (*Otx2, Mash1* and *Neurod1*) in control and GLE retinas, peaked mid-way of postnatal development at PN6. Moreover, in GLE *Otx2, Mash1, Rb1* and *p27 Cdkn1b* were significantly upregulated relative to control by 30% or more (Fig. 2m,n,o,p,q).

Molecular coupling of cell cycle exit and cell fate specification, and molecular uncoupling of these processes with cell cycle reentry in RPCs during development is suggested by the expression pattern of cell cycle regulators (cyclins, Inks, Cdks, Mcm6), which closely overlay with RPC cell cycle reentry temporal pattern (Fig. 1d), and expression pattern of regulators of cell cycle exit and differentiation overlap with RPC cell cycle exit and cell fate specification temporal pattern (Fig. 1e,i). For GLE these results suggest, GLE mediated upregulation of cell cycle activators (cyclins, Cdks, Mcm6, Hes1), downregulation of cell cycle inhibitors (Inks), cell cycle exit (p27) and neuronal cell fate specification factors (Ascl1, Otx2, Hes6), underlies and is consistent with the increased cell cycle reentry, cell cycle exit and neuronal cell fate specification of RPCs in GLE.

To gain greater developmental insight into spatiotemporal coupling and uncoupling or separation of regulators of cell cycle reentry, cell cycle exit and cell fate specification we performed immunohistochemistry. Moreover, we performed western blot analysis to quantify the protein expression levels and phosphorylation activation status of these molecular regulators. These results in control retina was compared with GLE to gain insights into the spatiotemporal and protein level GLE mediated changes to molecular regulators of cell cycle reentry, cell cycle exit and cell fate specification. In immunohistochemistry, RPCs were labeled with proliferation markers MCM6 or Ki67. These results and their conclusions are described below.

Spatiotemporal expression of CYCLINs during development is restricted to INBL during development and GLE upregulates expression of CYCLINs in RPCs.

Cell cycle progression requires sequential expression of CYCLINs that sequentially activate CDK phosphorylation activity (Levine and Green 2004). We found that CYCLIN D1 and CYCLIN A2 were localized in RPCs from PN2 to PN8. Their highest expression was at PN2 and labeled cells were present throughout the ONBL, but by PN6 with increasing age labeled cells were more pronounced in the proximal ONBL and INBL, the site of S phase, and gradually decreased until the SVZ, the site of M phase (Fig. 3a,b; Supp Fig. 2a,b). From PN2 to PN6 50-92% and 40-67% of the MCM6+RPCs colabeled with CYCLIN $D1^+$ and CYCLIN $A2^+$, respectively (Fig. 3a, b; Supp Fig. 2a,b). The difference between the GLE retinas relative to controls, was that the number of MCM6 and CYCLIN D1 or CYCLIN A2 colabeled cells increased by 27% to 68% (Fig. 3a,b; Supp Fig. 2a,b). Western blots and densitometry from PN2 to PN10 also showed an age dependent decrease in expression of CYCLIN D1, CYCLIN E2 and CYCLIN A2, and these cyclins were upregulated in GLE by 28-39% (Fig. 3c,d,e,f).

These result show that the expression of CYCLINs is predominantly in the INBL, the site of S-phase and the spatiotemporal expression pattern is similar to the laminar distribution of RPCs (MCM6+ cells), consistent with previous studies(Barton and Levine 2008). Both mRNA and protein expression of Cyclins is the same as the pattern of RPC cell cycle reentry (Fig. 1d). In GLE relative to control, the spatiotemporal expression pattern of CYCLINs is not altered, but an increased number RPCs express the CYCLINs, and the mRNA and protein expression of CYCLINs is higher in GLE, and is a molecular mechanism consistent with the GLE mediated accelerated cell cycle, increased cell cycle reentry, and cell cycle progression of RPCs.

CDK activity and RB1 hyperphosphorylation closely follows CYCLIN expression and RPC cell cycle entry pattern, and are upregulated in GLE.

Upregulation of cyclins are directly linked with increased activation of CDKs and subsequent hyperphosphorylation of RB which induces cell cycle reentry and progression by relieving E2F1 repression by RB1 (Bilitou and Ohnuma 2010). We found an age dependent decrease in expression of total CDKs (CDK4 and CDK2) and activated CDKs (pCDK2), proliferation marker (MCM6), RB and hyperphosphorylated RB1, p107 (RB family member) and E2F1 (Fig. 3c,g,h,i,j,k,l; Supp. Fig. 2f,g). These result show that both mRNA and protein expression of these cell cycle regulators, activity of CDKs and hyperphosphorylation is the same as the pattern of RPC cell cycle reentry (Fig. 1d). In GLE relative to control, we found an upregulation of expression (indicated in parentheses) in GLE of MCM6 (28-34%), CDK4 (34-41%), CDK2 (23-28%), RB1 (20-38%), activated CDK2 (pCDK2) (20-36%) and hyperphosphorylated RB1 (36-52%) (Fig. 3c,g,h,I,j,k,l; Supp. Fig. 2f,g). Thus, consistent with GLE induced increased expression of CYCLINs, there is increases activity of the cyclin dependent effector kinases, CDKs that in turn hyperphosphorylates RB1, an essential step for cell cycle progression, and is a molecular mechanism consistent with the GLE mediated accelerated cell cycle, increased cell cycle reentry, and cell cycle progression of RPCs.

Spatiotemporal expression of INKs during development is restricted to SVZ during development and GLE downregulates expression of INKs in RPCs.

p19 INK4d inhibit the activity of CDKs and are integral to cell cycle progression (Levine and Green 2004). We found that p16 INK4a+ (CDKN2A) and p19 INK4d+ (CDKN2D) spatiotemporal expression pattern was highest in the SVZ, where cells undergo mitosis, and the distal ONBL (Fig. 4a,b; Supp. Fig.2c,d). From PN2 to PN6 only 14% of the MCM6+ cells colabeled with p16 INK4a (Fig. 4a; Supp. Fig.2c). The age-dependent decrease in p16 INK4a and p19 INK4d, and their expression in RPCs is consistent with the age-dependent decrease in cell cycle. In GLE retinas the number of MCM6+RPCs colabeled with p16 INK4a decreased by 30%-52% relative to control (Fig. 4a; Supp. Fig.2c). The spatiotemporal expression of p19 INK4d appeared lower in GLE retinas compared to controls (Fig. 4b; Supp. Fig.2d). Western blot and densitometry from PN2 to PN10, confirmed the decreased expression of p16 INK4a and p19 INK4d with age in both GLE and control, and the downregulation of these genes in GLE by 20-27% relative to control (Fig. 4d,e,f). This shows that decreased p16 INK4a and p19 INK4d expression in RPCs by GLE underlies the molecular mechanism of increased cell cycle reentry and cell cycle progression of RPCs.

These result show that the expression of INKs is predominantly in the SVZ, the site of M-phase and the spatiotemporal expression pattern is opposite to the laminar distribution of CYCLIN+ RPCs in S-phase at the INBL (Fig. 3a,b). The spatiotemporal expression pattern of p19 is consistent to previous studies (Cunningham et al. 2002), while p16 spatiotemporal expression consistent had not been studies before. Both mRNA and protein expression of INKs is the same as the pattern of RPC cell cycle reentry (Fig. 1d), than cell cycle exit (Fig. 1e) and cell fate specification (Fig. 1i), which suggests that INKs may contribute more to cell cycle reentry. In GLE relative to control, the spatiotemporal expression pattern of INKs is not altered, but a decreased number RPCs express the INKs, and the mRNA and protein expression of INKs is lower in GLE, and is a molecular mechanism consistent with the GLE mediated accelerated cell cycle, increased cell cycle reentry, and cell cycle progression of RPCs.

p27 KIP1 is uniformly expressed spatiotemporal in SVZ and INBL during early development, and GLE upregulates expression of p27 KIP1 in RPCs.

p27 Kip1, inhibits cell cycle of RPCs to promote cell cycle exit in over 90% of RPCs exiting cell cycle in postnatal retina (Levine et al. 2000). Thus, differential regulation of p27 Kip1 is an indicator and regulator of RPC cell cycle exit. At PN2, p27 KIP1+ (CDKN1B+) cells were dispersed throughout the SVZ and ONBL, at PN4 they were highly expressed in the SVZ and distal ONBL, at PN6 they were in the SVZ, ONBL and INBL, and by PN8 they were exclusively located in Müller glial cells (Fig. 4c; Supp. Fig. 2e). At PN2 to PN6 only 28% of the MCM6+ cells colabeled with p27 KIP1 (Fig. 4c). Between GLE and control retinas the number of MCM6 and p27 KIP1 colabeled cells in GLE retinas, significantly increased at PN2 to PN6 by 126-87% (Fig. 4c; Supp. Fig. 2e). Western blot and densitometry from PN2 to PN10, showed that both control and GLE retinas had the same pattern of p27 KIP1 expression, but in GLE retinas p27 KIP1 expression significantly increased by 37% relative to control (Fig. 4d,g).

The pattern of p27 KIP1 expression (peak at PN4) and its colabeling with MCM6 is similar to the pattern of cell cycle exit, consistent with the role in promoting cell cycle

exit (Fig. 1e). At PN6 and PN8, the expression of p27 KIP1 intensifying in the INBL at the site of Müller glial cells location, consistent with previous results (Levine et al. 2000). The increased expression of p27 KIP1 and increased colabeling of p27 KIP1 with MCM6 is consistent with increased cell cycle exit in GLE. Thus, increase of p27 KIP1 expression is the molecular mechanism by which GLE increases cell cycle exit of RPCs.

Spatiotemporal expression of neuronal cell fate specification factors (OTX2, MASH1 and HES6) during development is restricted to SVZ and GLE specifically upregulates their expression without altering glial cell fate specification factors.

OTX2 and MASH1 are proneural factors that determine rod and bipolar cell fate (Nelson et al. 2009; Wang et al. 2014). From PN2 to PN4, the spatiotemporal expression of OTX2+ or MASH1+ and MCM6+RPCs colabeled cells were located in the outer retina in the SVZ and ONBL, and OTX2 appeared also in the INBL at PN6 (Fig. 5a,b; Supp. Fig.3a,b). Western blot and densitometry, corroborated these results and showed, expression peak of OTX2, MASH1, HES6 and NEUROD1 at PN4 during retinal development (Fig. 5c,d,e,f,g). In GLE retinas from PN2 to PN6 relative to control, there was 36% and 40% increase in OTX2 and MASH1 colabeled MCM6+RPCs, respectively without any change in spatiotemporal pattern of expression (Fig. 5a,b; Supp. Fig.3a,b). In GLE retinas relative to control, protein expression increased for OTX2 (28-44%), HES6 (31-36%) and MASH1 (14-52%) from PN2 to PN10 (Fig. 5c,d,f,g).

The pattern of OTX2, MASH1, NEUROD1 and HES6 expression (peak at PN4) and its colabeling with MCM6 is similar to the pattern of neuronal cell fate specification (Fig. 1i), consistent with their role in promoting neuronal cell fate specification. At PN6 and PN8, the expression of OTX2 intensifying in the INBL at the location of Muller glial cells has not been reported before and suggests potential non-neuronal functions of OTX2. Interestingly, the pattern of expression of cell cycle exit (Fig. 1e) and its regulator p27 KIP1 (Fig. 2e), and neuronal cell fate specification (Fig. 1i) and these neuronal cell fate regulators (OTX2 and MASH1) are spatiotemporally coupled, suggesting potential cooperation between these processes. In GLE relative to control, the increased expression of OTX2, MASH1 and HES6 and increased colabeling of OTX2 and MASH1 with MCM6 is consistent with increased neuronal cell fate specification in GLE. Thus, increase of OTX2, MASH1 and HES6 expression is the molecular mechanism by which GLE increases rod-bipolar neuronal cell fate specification and differentiation of RPCs.

Developmental age dependent switch in expression of NOTCH1 and HES1 from SVZ to INBL, and GLE differentially modulates NOTCH1 and HES1 activity.

The NOTCH1-HES1 pathway oscillatory expression promotes the proliferative expansion of the RPC pool and inhibits neuronal differentiation, whereas sustained expression of NOTCH1-HES1 pathway promotes glial cell fate (Balenci and van der Kooy 2014; Mizeracka et al. 2013; Nelson et al. 2009). At PN2 and PN4, NOTCH1 and HES1 expression was high in the SVZ and ONBL (Fig. 6a; Supp. Fig. 3c). From PN6 onwards, NOTCH1 and HES1 expression switched to high levels in INBL (Fig. 6a; Supp. Fig. 3c). The number of HES1 cells colabeled with RPCs significantly decreased from PN2 to PN8. In PN2 and PN4 almost all HES1+ cells colabeled with the Ki67+RPCs, 30% and 45% in control and GLE, respectively (Fig. 6a; Supp. Fig. 3c). By PN6, HES1+ and Ki67+ colabeling dramatically decreased by 15% in GLE relative to control (Fig. 6a; Supp. Fig.

3c). Western blot and densitometry, also showed an age dependent decrease in NOTCH1, NOTCH1-ICD (activated Notch1) and HES1 (Fig. 6b,c,d,e). In GLE retinas relative to controls from PN2 to PN4 there was increase in NOTCH1-ECD (25%), NOTCH1-ICD (30%) and HES1 (30%) consistent with increased proliferation, and all three proteins expression decreased by ~20% at PN6 in GLE consistent with completion of proliferation and increased neuronal cell fate specification (Fig. 6b,c,d,e). NOTCH1-HES1 also potentiates Muller glial cell fate specification through STAT3 activation, so we performed Western and densitometry in control and GLE retinas for STAT3 and p-STAT3 to determine if the activation of Notch1-Hes1 activated the glial pathway in GLE (Mizeracka et al. 2013). Both STAT3 and p-STAT3 (activated STAT3) expression increased from PN2 to PN4, and stayed high during the rest of the development. Between GLE and control there was no difference in STAT3 and p-STAT3 consistent with the fact that GLE does not change Muller glial cell fate (Fig. 6b,f,g).

These result show that the expression of NOTCH1-HES1 pathway is predominantly active in the SVZ, the site of M-phase. Both mRNA and protein expression of NOTCH1-HES1, and activated NOTCH1 (NOTCH1-ECD) is the same as the pattern of RPC cell cycle reentry (Fig. 1d), than cell cycle exit (Fig. 1e) and cell fate specification (Fig. 1i), which suggests that NOTCH1-HES1 pathway may contribute more to cell cycle reentry. Interestingly, there is no correlation in the pattern of NOTCH1-HES1 pathway and STAT3-pSTAT3 glial cell fate specification pathway, which suggests these pathways may have independent modes of glial cell fate specification in the postnatal retina. In GLE relative to control, the spatiotemporal expression pattern of NOTCH1-HES1 is not altered, but an increased number RPCs express the HES1, and the mRNA and protein expression of NOTCH1-HES1 is higher in GLE early on consistent with more cell cycle reentry, and lower in GLE later consistent with less cell cycle reentry and more neuronal cell fate specification, without change in Müller glial cell fate specification. Thus, NOTCH1-HES1 pathway modulation is a molecular mechanism consistent with the GLE mediated increased cell cycle reentry, and cell cycle progression of RPCs early on, and later with increased cell cycle exit and cell fate specification of RPCs. This shows that GLE mediated alteration in NOTCH1-HES1 pathway activity is a network hub of cross-talk between cell cycle and cell fate specification of RPCs.

GLE increases activity of the Cyclin D1 and Mash1 gene promoters.

We hypothesized that GLE increases recruitment of transcription factors at promoters of *Cyclin D1* and *Mash1* to upregulate their expression relative to control. To determine the transcriptional regulatory mechanisms underlying the GLE phenotype of simultaneously increased proliferation and rod photoreceptor, and neuronal cell fate specification, we investigated the recruitment of transcription factors by ChIP-qPCR on the *Cyclin D1* and *Mash1* promoter.

In both control and GLE retinas ChIP-qPCR showed that RNA POL2, E2F1 and C-JUN association at *CyclinD1* promoter was highest at PN2 and PN4, and decreased at PN6, (Fig. 7a,b,c). In GLE retinas there was increased recruitment of RNA POL2, E2F1, C-JUN and N-MYC relative to control (Fig. 7a,b,c). In control and GLE retinas, the relative binding of RNA POL2 and C-JUN to the *Mash1* promoter was highest at PN4, while that of E2F1 was highest at PN2 and PN4 (Fig. 7d,e,f). In GLE retinas

compared to controls, the relative binding activity of RNA-POL and C-JUN to the *Mash1* promoter increased from PN2-PN6, and E2F1 binding increased from PN2 to PN4 (Fig. 7d,e,f).

These results show that during development *Cyclin D1* and *Mash1* share transcription factors (RNA POL2, E2F1, C-JUN, N-MYC), which provides a point of coordination between cell cycle and neuronal cell fate specification, and the occupancy of their promoters decreases at PN6 with exhaustion of RPCs and completion of cell cycle and cell fate specification. In GLE the increased binding of key transcription factors to the *CyclinD1* and *Mash1* promoters is consistent with increased proliferation and rod-bipolar differentiation .

DISCUSSION

This study has revealed more of the complexity of coordination of cell cycle, cell cycle exit and cell fate specification processes and their molecular regulators in RPCs during retinal development (Fig. 7g,h). We show several lines of evidence to show strong coupling between temporal pattern of number of RPC undergoing cell cycle exit and neuronal cell fate specification, and temporal expression pattern of molecular regulators of cell cycle exit (p27 KIP1) and neuronal cell fate specification (ASCL1, OTX2, NEUROD1, HES6). Temporal expression pattern of molecular regulators of cell cycle, the inhibitors (p16 INK4a, p16 INK4d), CDK activity (pRB, pCDK4), NOTCH1-HES1 pathway proteins and cyclins (CYCLIN D1, A2, E1) showed strong coupling with temporal pattern of number of RPCs undergoing cell cycle reentry. These results show that expression pattern is a good indicator of molecular function and RPC phenotypic outcome.

Timing of cell fate specification in RPCs by neuronal cell fate specification factors and the role of cell cycle inhibitors in cell fate specification in RPCs has been a long-standing question. The cell cycle inhibitors, p57KIP2 and p27KIP1 expression in RPCs induce cell cycle exit in embryonic and postnatal RPCs, respectively (Dyer and Cepko 2001), while among INKs, p19INK4d expresses with p27KIP1 in RPCs to potentiate cell cycle exit (Cunningham et al. 2002). Additionally, p27KIP1 also promotes Müller glial cell fate of RPCs and p27KIP1 levels are maintained high in Müller glial cells (Levine et al. 2000), but if the INKs play any role in cell fate specification is unknown. Our results, show that p16INK4a and p19INK4d expression pattern is spatially localized with p27KIP1 and neuronal factors (OTX2, MASH1) in SVZ RPCs and postmitotic cells, which supports the possible role of INKs in cell cycle exit and cell fate specification in RPCs (Fig. 7g,h). The known mechanism of action of cell cycle inhibitors is by blocking CYCLIN-CDK complex kinase activity, but how p27KIP1 and potentially INKs regulate cell fate specification requires further study. Expression of neuronal factor NGN2 in subset of embryonic RPCs primes them for ganglion neuron cell fate, while MASH1 expression in subset of embryonic RPCs primes them to other neuronal cell fates (Brzezinski et al. 2011). The potential mechanism of action of neuronal cell fate specification factors in RPCs is through transcriptional regulation, and it has been shown that MASH1 directly regulate cell cycle genes in addition to its canonical neuronal target genes and in embryonic brain and neural stem cell culture (Castro et al. 2011). The RPC priming by neuronal cell fate transcription factors, such as MASH1 is different from classical cell fate specification that occurs in RPCs by expression of the

neuronal cell fate transcription factors. A primed RPC should in principle undergo one or two rounds of cell cycle before cell fate specification terminal differentiation. Our results, show that neuronal factors, MASH1 and OTX2 expression pattern is spatially localized with p27KIP1 and INKs (p16 INK4a, p19INK4d) in SVZ RPCs and postmitotic cells (Fig. 7g,h). Importantly, we did not observe MASH1+ RPCs or OTX2+ RPCs in INBL, which would have appeared had RPCs been primed and continued to cycle atleast once before cell fate specification. These results support the idea that MASH1 and OTX2 predominantly play a role in cell fate specification at the end of terminal differentiation in postnatal RPCs and not in RPC neuronal cell fate priming. Another, possible explanation is that in our studies which were in postnatal retina, MASH1 mediated RPC priming does not occur, while priming of RPCs by MASH1 is a process that occurs in embryonic retina the timepoint for the previous study that showed MASH1 mediated RPC priming(Brzezinski et al. 2011). More research is required to resolve the context of MASH1, OTX2 and other neuronal cell fate specification factors in RPCs.

The NOTCH1-HES1 pathway is the master positive regulator of proliferation and glial cell fate, and actively inhibits neuronal cell fate (Zhou et al. 2010). In the present study, we show that NOTCH1 and HES1 are spatially localized to the SVZ and ONBL in RPC and postmitotic cells, similar to cell cycle inhibitors (p27KIP1, p16 INK4a, p19 INK4d) and neuronal cell fate specification factors (OTX2, MASH1), while cell cycle activator cyclin expression was spatially separated localized to the INBL in RPC and few postmitotic cells (Fig. 7g,h). During cell cycle the RPC cell bodies move between INBL, site of S phase to SVZ, site of M phase, while G1 and G2 phases occur in between SVZ and INBL (Baye and Link 2007). Taken together these results suggest that the decisions for cell cycle reentry, cell cycle exit and cell fate specification are being taken in the RPCs in the SVZ, and the molecular cascade regulating these processes (p27 KIP, INKs, OTX2, MASH1) are potentially being inhibited by NOTCH1-HES1 in RPCs to promote cell cycle reentry in RPCs. NOTCH1-HES1 pathway can inhibit p27 KIP1 in different developmental tissues (Murata et al. 2005), MASH1 in central nervous system (Kageyama and Ohtsuka 1999) and activate CYCLIN D1 in lens (Rowan et al. 2008). Interestingly, we did not find a major NOTCH1-HES1 expression in RPCs in INBL where CYCLINs are highly expressed in RPCs, which suggested that once the RPC decide to reenter cell cycle under NOTCH1-HES1 regulation in SVZ and ONBL, the regulation of cell cycle progression is regulated by CYCLINs and does not require sustained expression of NOTCH1-HES1 in INBL. In future studies, it remains to be seen if in the retina NOTCH1-HES1 pathway regulates INKs, OTX2 and other neuronal specification factors, and CYCLINs. It is known that RPCs mainly divide asymmetrically in postnatal retina (Kechad et al. 2012) and asymmetrically dividing progenitor cells are known to asymmetrically distribute molecular regulators (Roegiers and Jan 2004). At PN4 we observe almost equal number of RPCs reentering cell cycle, and exiting cell cycle and undergoing cell fate specification. These results further suggest that RPCs divide asymmetrically to generate two daughter cells, one rich in NOTCH1-HES1, and another rich in cell cycle inhibitors (p27 KIP1, INKs) and neuronal cell fate specification factors (MASH1, OTX2), resulting in a peak of both proliferating RPCs and differentiating RPCs at PN4. As finding primary antibodies from different species is challenging to do colabeling studies of all these regulators, it is hoped that in future single cell RNA-seq of RPCs from PN4 retinas, to understand the frequency of

combination of these and other molecular regulators that RPCs utilize to undergo cell cycle reentry, cell cycle exit and cell fate specification.

In this study, we have found a novel molecular mechanism of cell cycle, cell cycle exit and cell fate specification factors (Fig. 7g,h) underlying the previously reported novel GLE phenotype of increased proliferation and neuronal cell fate specification in the retina, without change in apoptosis (Giddabasappa et al. 2011). The cellular mechanism to cause this novel GLE phenotype could be sequential or concurrent increase in RPC proliferation and RPC differentiation into rod photoreceptor and bipolar neurons. Analysis of cell cycle dynamics and differentiation dynamics of RPCs using BrdU and other cellular markers, we found that GLE induced a concurrent increase in RPCs reentering cell cycle, and undergoing cell cycle exit and cell fate specification or differentiation. It is known that during normal development, shortening of cell cycle length causes increase in cell cycle reentry of RPCs at the expense of cell fate specification (Alexiades and Cepko 1996; Takahashi et al. 1993). Surprisingly, we found that GLE accelerated cell cycle by shortening the length of G1 phase of cell cycle without changing the ratio of RPCs undergoing cell cycle reentry and cell cycle exit, and cell fate specification. This raised the question, how does GLE balance the normal developmental force of decreased cell fate specification of RPCs with an increase in cell cycle reentry of RPCs when shortening of cell cycle length occurs. The G1 phase consists of an early G1 phase before the restriction point, when RPCs are not committed to reenter cell cycle and a late G1 phase closer to S phase when RPCs are committed to reenter cell cycle (Johnson and Skotheim 2013). Thus, it is possible that in the early G1 phase the RPCs can exit cell cycle to differentiate, while in the late G1 phase RPCs are committed to cell cycle progression. Therefore, we hypothesized that GLE shortens both the early G1 phase length to accelerate developmental commitment decisions of RPCs to undergo cell cycle exit and cell fate specification of RPCs, and shortens the late G1 phase to accelerate developmental commitment decisions of RPCs to undergo cell cycle progression. We took advantage of the known interkinetic movement and localization of RPCs in different phases of cell cycle, whereby early G1 phase RPCs are likely to be near M phase cells in SVZ and ONBL, while late G1 phase RPCs are likely to be near S phase cells in the INBL (Baye and Link 2007). In support of our hypothesis, in GLE relative to control we found that SVZ and ONBL localized p16 INK4a and p19 INK4d were downregulated, consistent with shortening of cell cycle in early G1 phase RPCs, while INBL localized CYCLINs (CYCLIN D1, A2, potentially E2) were upregulated, consistent with shortening of cell cycle in late G1 phase RPCs. Other studies have shown that accumulation of CDK inhibitors in developmental neurogenesis slows down G1 phase length (Hindley and Philpott 2012), while CYCLIN D1 accelerates G1 phase length in retina (Das et al. 2009) also support this molecular mechanism of GLE mediated cell cycle length control.

As noted earlier, we found that GLE shortens cell cycle and increases number of RPCs undergoing cell cycle reentry, cell cycle exit and cell fate specification, without changing the ratio of RPCs undergoing cell cycle reentry, cell cycle exit and cell fate specification. Thus, in GLE relative to control RPCs are required to quickly make decisions of cell cycle reentry, cell cycle exit and cell fate specification such that the number increases but the ratio of RPCs undergoing cell cycle reentry, cell cycle exit and cell fate specification does not change. We found the molecular mechanism by which

GLE coordinates this phenotype by Affymetrix gene expression array and validation of differentially expressed target genes in GLE relative to control retinas. GLE simultaneously upregulated molecular regulators of RPC cell cycle reentry (NOTCH1-HES1 pathway), cell cycle progression (Cdks, Notch1-Hes1 activity, Cdk4 phosphorylation, Rb phosphorylation), cell cycle exit (p27 Cdkn1b) and neuronal cell fate specification (Otx2, Mash1, Hes6) of RPCs, without changing their spatiotemporal expression pattern. It is still unclear if these diverse molecular changes in regulators of cell cycle progression, cell cycle exit and neuronal cell fate regulation are an indirect effect of GLE resulting from shortening of G1 phase length by GLE mediated altered expression of Cyclins and INKs, or a direct effect of GLE. Moreover, it is possible that these diverse molecular regulators of cell cycle progression, cell cycle exit and neuronal cell fate regulation, also play a role in regulation of cell cycle length at early and late G1 phase. Evidence in support of a direct cell cycle length independent mechanism for regulation of cell cycle progression, cell cycle exit and neuronal cell fate by GLE is supported by the finding that GLE does not change glial cell fate specification factors (STAT3, p-STAT3) or number of Muller glial cells. If the GLE phenotype was only a result of regulation of cell cycle length, then all cell fates neuronal and glial would be increased, but in GLE we only see a specific increase in neuronal cell fate factors (OTX2, MASH1). Furthermore, we show that GLE increases the occupancy of c-JUN, a known direct interactor of Pb (Ramesh et al. 1999), on active promoters of Cyclin D1 and Mash1 GLE dependent genes that regulate cell cycle length/progression and neuronal cell fate specification. These findings document the molecular mechanisms by which GLE specifically and directly regulates, G1 phase cell cycle length, cell cycle reentry, cell cycle progression, cell cycle exit and neuronal cell fate specification, but not glial cell fate specification (Fig. 7g,h).

Our findings in RPCs point to a novel effect of lead on neural progenitor cells of cell cycle acceleration. This contrasts with other studies that have shown that lead exposure slows down and impairs proliferation of neural progenitor cells in the hippocampus (Gilbert et al. 2005; Schneider et al. 2005; Verina et al. 2007). One possible reason for the difference could be because there are tissue specific differences between retina and hippocampus, which results in different handling of lead. Another, explanation for the difference is that in the GLE model the lead dose is low or moderate, while the other hippocampus lead exposure models utilize a higher and chronic dose of lead. Lymphocytes are not progenitor cells, but can proliferate to produce T-cells and B-cells for immune response of the body. In lymphocytes, lead had a stimulatory effect on proliferation at low dose, which again shows the importance of lead exposure level in determining the phenotypic outcome of lead exposure (Razani-Boroujerdi et al. 1999). Taken together these results suggest that the effect of lead on proliferation depends on the context of tissue, timing and level of exposure.

Given the context dependent effect of lead on proliferation of progenitor cells, it maybe expected that at the molecular level the target genes of lead will be context dependent. In the context of GLE, we found upregulation of positive regulators of cell cycle (NOTCH1-HES1, and CYCLINs), cell cycle exit (p27 KIP1) and rod photoreceptor, and bipolar cell differentiation (OTX2, MASH1 and HES6), while GLE downregulated cell cycle inhibitors (p16 INK4a and p19 INK4d). A recent study showed that in the context of higher lead exposure (1mM lead acetate trihydrate) in culture media neural

stem cells induces oxidative stress response gene Nrf2 (Wagner et al. 2017) consistent with impaired proliferation, while in lymphocytes low levels of lead activated proliferation by enhancing cell-cell contact and IP3 signaling (Razani-Boroujerdi et al. 1999). Low levels of lead exposure induced hepatocyte proliferation in liver by TNFα signaling (Columbano et al. 1983; Kubo et al. 1996). These results demonstrate that similar to the phenotypic effect of lead on progenitor cells, the molecular pathways induced by lead exposure is context dependent.

Calcium signaling is a well-known context dependent regulator of cell cycle and differentiation of progenitor cells (Carafoli 2002; Ducibella et al. 2006; Orrenius et al. 2003). Several studies have shown that lead can “hijack” calcium signaling pathways to induce toxic effects (Fox and Katz 1992; He et al. 2000; Simons 1993). One study showed that lead mediated proliferation effects in smooth muscle is rescued by calcium ionophore A23187, which suggests cross-talk between lead and calcium signaling pathways (Fujiwara et al. 1995). More research is needed to investigate the extend of overlap between lead and calcium signaling, which could help understand how lead plays a wide variety of context dependent roles in progenitor cells. The list of differentially expressed GLE induced genes we have described will provide a foundation for the development of new biomarkers of low dose lead toxicity (Fox et al. 2010). Studies have shown that human and rodent models are in good agreement in toxicology studies (Culbreth et al. 2012), which supports that our GLE results in mouse model should be translatable to human GLE. We also propose that for in vitro or in vivo heavy metal screening assays progenitor cells can be a great tool as a wide-variety of phenotypes and molecular mechanisms that range from cell cycle to cell death can be assayed using progenitor cells. Moreover, in studies of lead and other heavy metals, especial care should be taken on the dose, target cell type, time and duration of exposure.

FIGURE LEGENDS

Figure 1: Developmental pattern of cell cycle reentry, cell cycle exit and cell fate specification and cell cycle phase lengths in RPCs. GLE induced accelerated cell cycle, increased cell cycle entry, cell cycle exit and cell fate specification. a) Gestational lead exposure model of mice. Female mice were exposed to lead through their drinking water for 14 days prior to conception to establish a steady-state blood lead level before mating. After mating, dams were exposed to lead throughout gestation and exposure was continued from birth PN0 until PN10. This GLE model ensures that mice were exposed to lead for a period equivalent to the duration of human gestation. b-j) In mice that were injected with a single pulse of 24 hours before sacrificing for immunohistochemistry and graphical analysis of BrdU with MCM6 (b) and OTX2 (g) revealed increased number of RPCs BrdU+ (c), increased MCM6+BrdU+ cell cycle entry (d), increased MCM6-BrdU+ cell cycle exit (e), increased OTX2+BrdU+ neuronal cell fate specification in RPCs (i) and increased postmitotic neurons OTX2+ (h) in GLE. d,f) Number and ratio of RPCs reentering cell cycle decreased with age in control and GLE retinas. e,f,I,j) Number of RPCs exiting cell cycle and undergoing neuronal cell fate specification peaked at PN4 and then decreased with age, while the ratios decreased steadily with age in control and GLE retinas. Plots and graphical analysis of the labeling index vs survival time obtained from cumulative BdrU labeling and Draq5 staining reveals the total cell cycle length (Tc) as 32 hrs in control and 24 hrs in GLE, S phase length (Ts) 11.5 hrs and growth fraction (GF) as 0.55 in both. The composite results from these cell cycle experiments enabled the determination of cell cycle entry phase length [cell cycle entry = Tc – Ts – (G2+M)] and revealed that GLE selectively decreased the cell cycle entry phase of the cell cycle. For all quantifications data are plotted as the mean±sem, *p<0.05 and scale bar = 40 µm. Also see Supplementary Figure 1.

Figure 2: Effect of GLE on postnatal retina gene expression using the Affymetrix platform. a) Bar graph shows number of significant differentially expressed genes and Gene Ontology (GO) of these genes between GLE and control retinas. b) Heatmap presentations of genes from GOs “cell cycle” and “neuronal differentiation” expression levels measured by Affymetrix probe sets among differentially expressed between GLE and control retinas. qPCR validation of candidate “cell cycle” genes. c-m) Cell cycle activators *CyclinD1*(c), *CyclinE1*(d), *CyclinA2*(e) and cell cycle regulators/markers *Mcm6*(f), *Cdk4*(g), *Cdk2*(h), were upregulated in GLE. *Hes1*(i) and *Hes6*(j) were upregulated in GLE. Cell cycle inhibitors *p16 Ink4a*(k) and p19 Ink4d(l) were downregulated in GLE. Cell cycle regulator *Rb1*(m) and cell fate specification factor *p27 Kip1*(n) were upregulated in GLE. qPCR validation of candidate “neuronal differentiation” genes. o-q) Proneuronal rod-bipolar cell fate specification and differentiation factors, *Otx2*(o) and *Mash1*(p) were upregulated in GLE, but there was no change in *Neurod1*(q). For all quantifications data are plotted as the mean±sem, *p<0.05.

Figure 3: Expression of CYCLINs decreases with development age and is GLE upregulated by GLE. Immunolabeling of CYCLIN D1(a) and CYCLIN A2(b) are highest in S-phase RPCs in INBL and present in RPCs in SVZ of GLE and control retinas. However, in GLE retinas the number of these cyclin colabeled RPCs was increased. c-l)

Quantification by western blot and densitometry show age dependent decreased expression of cell cycle proteins, CYCLIN D1(c,d), CYCLIN E2(c,e), CYCLIN A2(c,f), MCM6(c,g), RB1(c,h), pRB1(c,i), CDK4(c,j), CDK2(c,k) and pCDK2(c,l) consistent with completion of development in control and GLE retinas. In GLE expression of all these cell cycle proteins, was upregulated. These results are consistent with increased cell cycle progression and cell cycle entry in GLE relative to control. For all quantifications data are plotted as the mean±sem, *p<0.05. Scale bar = 40 µm. Also, see Supplementary Figure 2.

Figure 4: Expression of INKs decreases with developmental age and p27 KIP1 expression peaks at PN4. GLE downregulates expression of INKs and upregulates expression of p27 KIP1. Immunolabeling of cell cycle inhibitors p16 INK4a(a) and p19 INK4d(b), and cell cycle exit regulator p27 KIP1(c) are highest in RPCs in SVZ of GLE and control retinas. However, in GLE retinas the number of these cell cycle inhibitor p16 INK4a and p19 INK4d colabeled RPCs was decreased, while p27 KIP1 cell cycle exit regulator colabeled RPCs was increased. d-g) Quantification by western blot and densitometry show age dependent decreased expression of cell cycle inhibitor proteins, p16 INK4a(d,e) and p19 INK4d(d,f) consistent with completion of development, and peak of cell cycle exit regulator p27 KIP1(d,g) consistent with peak of cell cycle exit/cell fate specification in control and GLE retinas. In GLE expression of p16 INK4a and p19 INK4d was downregulated, while that of p27 KIP1 was upregulated. These results are consistent with increased cell cycle progression, cell cycle entry and cell cycle exit in GLE relative to control. For all quantifications data are plotted as the mean±sem, *p<0.05. Scale bar = 40 µm. Also, see Supplementary Figure 2.

Figure 5: Expression of MASH1 increases with developmental age, while OTX2, NEUROD1 and HES6 peak at PN4. GLE upregulates expression of MASH1, OTX2 and HES6. Imunolabeling of OTX2(a) and MASH1(b) are highest in the SVZ RPCs where cell cycle exit and cell fate specification occurs in control and GLE retinas. However, in GLE retinas the number of OTX2 and MASH1 colabeled RPCs was increased. c-g) Quantification by western blot and densitometry shows peak expression at PN4 of cell fate specification factors OTX2(c,d), NEUROD1(c,e), HES6(c,f) and MASH1(c,g) consistent with peak of cell cycle exit and rod-bipolar cell fate specification in control and GLE retinas. In GLE expression of all OTX2, HES6 and MASH1 were upregulated, while NEUROD1 did not change. For all quantifications data are plotted as the mean±sem, *p<0.05. Scale bar = 40 µm. Also see Supplementary Figure 3.

Figure 6: Expression and activation of NOTCH1-HES1 pathway decreases with developmental age, while STAT3 activation peaks and sustains after PN4. GLE differentially regulates Notch1-Hes1 pathway to maintain RPCs early on and make RPCs permissive for differentiation at PN6. a) Immunolabeling of NOTCH1, HES1 and Ki67 shows that early on at PN2 there is more colabeling of RPCs with HES1 and more labeling of Notch in SVZ in control and GLE retinas consistent with role of NOTCH1-HES1 pathway in maintenance or cell cycle entry of RPCs. This colabeling of HES1 RPC colabeling was increased in GLE. At PN6 HES1 and Ki67 were localized in inner retina but did not colabel (HES1 is known to express in Müller glial cells at this age). b-g)

Quantification by western blot and densitometry show age dependent decreased expression of NOTCH1(b,c), NOTCH1 activation (NOTCH1-ICD)(b,d) and HES1(b,e) consistent with completion of development in control and GLE retinas. Müller glial cell fate specification factors STAT3(f) and pSTAT3(g) peaked and stayed up PN6 onwards in control and GLE retinas, overlapping with known Muller glial cell specification timing. In GLE expression of all NOTCH1-HES1, was upregulated upto PN4 supporting increased cell cycle entry of RPCs and went down PN6 onwards making it permissive to rod-bipolar cell fate specification. Interestingly, STAT3 and pSTAT3 did not change in GLE consistent with no change in Muller glial cell number in GLE. For all quantifications data are plotted as the mean±sem, *p<0.05. Scale bar = 40 μm. Also see Supplementary Figure 3.

Figure 7: Developmental age and GLE dependent transcription factor occupancy on CyclinD1 and Mash1 promoters. Summary model. ChIP-qPCR was performed to evaluate the binding and activity of CyclinD1 and Mash1 promoter. a-c) In control and GLE retinas, RNA POL2 and E2F1 exhibited significant age-dependent decreases in relative binding to CyclinD1-promoter from PN2-PN4 to PN6. GLE increases the relative binding of RNA POL2, E2F1 and C-JUN at PN2 and PN4, while N-MYC binding increases in GLE at PN4 only. d-f) In control and GLE PN2-PN6 retinas, RNA POL2 and C-JUN exhibited significant binding peaks to Mash1 at PN4, while E2F1 exhibited significantly high binding to Mash1 at PN2 and PN4. Furthermore, in GLE retinas the relative binding of RNA POL2 and C-JUN significantly increased from PN2 to PN4, whereas E2F1 binding significantly increased at PN2 and PN4. g) Summary of spatial distribution of cell cycle regulators (CYCLINs, INKs), cell cycle exit regulator p27 KIP1, neuronal cell fate specification factors (MASH1, OTX2) and NOTCH1-HES1 RPC self-renewal pathway in SVZ, ONBL and INBL of developing postnatal retina. Intensity of color is directly proportional to expression level, and checkered pattern specifically indicates switched expression pattern at PN6. h) Summary model for cell cycle reentry, cell cycle exit and neuronal cell fate specification. CYCLINs and INKs regulate CDK activity and RB phosphorylation, which determines number of RPCs cell cycle entry in retina. GLE upregulates CYCLINs and downregulates INKs to increase cell cycle entry, cell cycle progression and shorten length of G1 phase of cell cycle. NOTCH1-HES1 pathway, p27 and MASH1, regulate the number of RPCs that exit cell cycle to acquire rod and bipolar cell fate. Moreover, these results suggest that GLE alters NOTCH1-HES1 pathway and G00sp Otx2, Hes6 and Mash1 and cell cycle exit factor p27 to increase neurogenesis of rod and bipolar cells. For all quantifications data are plotted as the mean±sem, *p<0.05.

REFERENCES

Ahmad I, Dooley CM, Afiat S. 1998. Involvement of mash1 in egf-mediated regulation of differentiation in the vertebrate retina. Developmental biology 194:86-98.

Alexiades MR, Cepko C. 1996. Quantitative analysis of proliferation and cell cycle length during development of the rat retina. Developmental dynamics : an official publication of the American Association of Anatomists 205:293-307.

Bae S, Bessho Y, Hojo M, Kageyama R. 2000. The bhlh gene hes6, an inhibitor of hes1, promotes neuronal differentiation. Development 127:2933-2943.

1064 Balenci L, van der Kooy D. 2014. Notch signaling induces retinal stem-like properties in
1065 perinatal neural retina progenitors and promotes symmetric divisions in adult retinal
1066 stem cells. Stem cells and development 23:230-244.
1067 Barton KM, Levine EM. 2008. Expression patterns and cell cycle profiles of pcna,
1068 mcm6, cyclin d1, cyclin a2, cyclin b1, and phosphorylated histone h3 in the developing
1069 mouse retina. Developmental dynamics : an official publication of the American
1070 Association of Anatomists 237:672-682.
1071 Basha MR, Wei W, Bakheet SA, Benitez N, Siddiqi HK, Ge YW, et al. 2005. The fetal
1072 basis of amyloidogenesis: Exposure to lead and latent overexpression of amyloid
1073 precursor protein and beta-amyloid in the aging brain. The Journal of neuroscience : the
1074 official journal of the Society for Neuroscience 25:823-829.
1075 Baye LM, Link BA. 2007. Interkinetic nuclear migration and the selection of neurogenic
1076 cell divisions during vertebrate retinogenesis. The Journal of neuroscience : the official
1077 journal of the Society for Neuroscience 27:10143-10152.
1078 Baye LM, Link BA. 2008. Nuclear migration during retinal development. Brain Res
1079 1192:29-36.
1080 Bellinger DC. 2008. Neurological and behavioral consequences of childhood lead
1081 exposure. PLoS medicine 5:e115.
1082 Bilitou A, Ohnuma S. 2010. The role of cell cycle in retinal development: Cyclin-
1083 dependent kinase inhibitors co-ordinate cell-cycle inhibition, cell-fate determination and
1084 differentiation in the developing retina. Developmental dynamics : an official publication
1085 of the American Association of Anatomists 239:727-736.
1086 Brzezinski JAt, Kim EJ, Johnson JE, Reh TA. 2011. Ascl1 expression defines a
1087 subpopulation of lineage-restricted progenitors in the mammalian retina. Development
1088 138:3519-3531.
1089 Canfield RL, Henderson CR, Jr., Cory-Slechta DA, Cox C, Jusko TA, Lanphear BP.
1090 2003. Intellectual impairment in children with blood lead concentrations below 10 microg
1091 per deciliter. The New England journal of medicine 348:1517-1526.
1092 Carafoli E. 2002. Calcium signaling: A tale for all seasons. Proceedings of the National
1093 Academy of Sciences of the United States of America 99:1115-1122.
1094 Castro DS, Martynoga B, Parras C, Ramesh V, Pacary E, Johnston C, et al. 2011. A
1095 novel function of the proneural factor ascl1 in progenitor proliferation identified by
1096 genome-wide characterization of its targets. Genes & development 25:930-945.
1097 Cepko C. 2014. Intrinsically different retinal progenitor cells produce specific types of
1098 progeny. Nature reviews Neuroscience 15:615-627.
1099 Chaney SY, Mukherjee S, Giddabasappa A, Rueda EM, Hamilton WR, Johnson JE, Jr.,
1100 et al. 2016. Increased proliferation of late-born retinal progenitor cells by gestational
1101 lead exposure delays rod and bipolar cell differentiation. Molecular vision 22:1468-1489.
1102 Chenn A, Walsh CA. 2002. Regulation of cerebral cortical size by control of cell cycle
1103 exit in neural precursors. Science 297:365-369.
1104 Columbano A, Ledda GM, Sirigu P, Perra T, Pani P. 1983. Liver cell proliferation
1105 induced by a single dose of lead nitrate. The American journal of pathology 110:83-88.
1106 Cordova FM, Rodrigues AL, Giacomelli MB, Oliveira CS, Posser T, Dunkley PR, et al.
1107 2004. Lead stimulates erk1/2 and p38mapk phosphorylation in the hippocampus of
1108 immature rats. Brain Res 998:65-72.

1109 Culbreth ME, Harrill JA, Freudenrich TM, Mundy WR, Shafer TJ. 2012. Comparison of
1110 chemical-induced changes in proliferation and apoptosis in human and mouse
1111 neuroprogenitor cells. Neurotoxicology 33:1499-1510.
1112 Cunningham JJ, Levine EM, Zindy F, Goloubeva O, Roussel MF, Smeyne RJ. 2002.
1113 The cyclin-dependent kinase inhibitors p19(ink4d) and p27(kip1) are coexpressed in
1114 select retinal cells and act cooperatively to control cell cycle exit. Molecular and cellular
1115 neurosciences 19:359-374.
1116 Das G, Choi Y, Sicinski P, Levine EM. 2009. Cyclin d1 fine-tunes the neurogenic output
1117 of embryonic retinal progenitor cells. Neural development 4:15.
1118 Dobbing J, Sands J. 1979. Comparative aspects of the brain growth spurt. Early human
1119 development 3:79-83.
1120 Ducibella T, Schultz RM, Ozil JP. 2006. Role of calcium signals in early development.
1121 Seminars in cell & developmental biology 17:324-332.
1122 Dyer MA, Cepko CL. 2001. P27kip1 and p57kip2 regulate proliferation in distinct retinal
1123 progenitor cell populations. The Journal of neuroscience : the official journal of the
1124 Society for Neuroscience 21:4259-4271.
1125 Fox DA, Katz LM. 1992. Developmental lead exposure selectively alters the scotopic
1126 erg component of dark and light adaptation and increases rod calcium content. Vision
1127 research 32:249-255.
1128 Fox DA, Campbell ML, Blocker YS. 1997. Functional alterations and apoptotic cell death
1129 in the retina following developmental or adult lead exposure. Neurotoxicology 18:645-
1130 664.
1131 Fox DA, Kala SV, Hamilton WR, Johnson JE, O'Callaghan JP. 2008. Low-level human
1132 equivalent gestational lead exposure produces supernormal scotopic
1133 electroretinograms, increased retinal neurogenesis, and decreased retinal dopamine
1134 utilization in rats. Environ Health Perspect 116:618-625.
1135 Fox DA, Opanashuk L, Zharkovsky A, Weiss B. 2010. Gene-chemical interactions in the
1136 developing mammalian nervous system: Effects on proliferation, neurogenesis and
1137 differentiation. Neurotoxicology 31:589-597.
1138 Fox DA, Boyes WK. 2013. Toxic responses of the ocular and visual system. In: CD
1139 Klaassen, JB Watkins (Eds), Casarett & Doull's Essentials of Toxicology, 8th Edition,
1140 McGraw-Hill Press, New York, USA:767-798.
1141 Fox DA. 2015. Retinal and visual system: Occupational and environmental toxicology.
1142 Handbook of clinical neurology 131:325-340.
1143 Freire P, Vinod PK, Novak B. 2012. Interplay of transcriptional and proteolytic regulation
1144 in driving robust cell cycle progression. Molecular bioSystems 8:863-870.
1145 Fujiwara Y, Kaji T, Yamamoto C, Sakamoto M, Kozuka H. 1995. Stimulatory effect of
1146 lead on the proliferation of cultured vascular smooth-muscle cells. Toxicology 98:105-
1147 110.
1148 Fukuda S, Taga T. 2005. Cell fate determination regulated by a transcriptional signal
1149 network in the developing mouse brain. Anatomical science international 80:12-18.
1150 Furukawa T, Mukherjee S, Bao ZZ, Morrow EM, Cepko CL. 2000. Rax, hes1, and
1151 notch1 promote the formation of muller glia by postnatal retinal progenitor cells. Neuron
1152 26:383-394.
1153 Giddabasappa A, Hamilton WR, Chaney S, Xiao W, Johnson JE, Mukherjee S, et al.
1154 2011. Low-level gestational lead exposure increases retinal progenitor cell proliferation

1155 and rod photoreceptor and bipolar cell neurogenesis in mice. Environmental Health
1156 Perspectives 119:71-77.
1157 Gilbert ME, Kelly ME, Samsam TE, Goodman JH. 2005. Chronic developmental lead
1158 exposure reduces neurogenesis in adult rat hippocampus but does not impair spatial
1159 learning. Toxicological sciences : an official journal of the Society of Toxicology 86:365-
1160 374.
1161 Goureau O, Rhee KD, Yang XJ. 2004. Ciliary neurotrophic factor promotes muller glia
1162 differentiation from the postnatal retinal progenitor pool. Developmental neuroscience
1163 26:359-370.
1164 Gratton MO, Torban E, Jasmin SB, Theriault FM, German MS, Stifani S. 2003. Hes6
1165 promotes cortical neurogenesis and inhibits hes1 transcription repression activity by
1166 multiple mechanisms. Molecular and cellular biology 23:6922-6935.
1167 Hatakeyama J, Kageyama R. 2004. Retinal cell fate determination and bhlh factors.
1168 Seminars in cell & developmental biology 15:83-89.
1169 He L, Poblenz AT, Medrano CJ, Fox DA. 2000. Lead and calcium produce rod
1170 photoreceptor cell apoptosis by opening the mitochondrial permeability transition pore.
1171 The Journal of biological chemistry 275:12175-12184.
1172 He L, Perkins GA, Poblenz AT, Harris JB, Hung M, Ellisman MH, et al. 2003. Bcl-xl
1173 overexpression blocks bax-mediated mitochondrial contact site formation and apoptosis
1174 in rod photoreceptors of lead-exposed mice. Proceedings of the National Academy of
1175 Sciences of the United States of America 100:1022-1027.
1176 Hindley C, Philpott A. 2012. Co-ordination of cell cycle and differentiation in the
1177 developing nervous system. The Biochemical journal 444:375-382.
1178 Hodge RD, D'Ercole AJ, O'Kusky JR. 2004. Insulin-like growth factor-i accelerates the
1179 cell cycle by decreasing g1 phase length and increases cell cycle reentry in the
1180 embryonic cerebral cortex. The Journal of neuroscience : the official journal of the
1181 Society for Neuroscience 24:10201-10210.
1182 Jadhav AP, Cho SH, Cepko CL. 2006a. Notch activity permits retinal cells to progress
1183 through multiple progenitor states and acquire a stem cell property. Proceedings of the
1184 National Academy of Sciences of the United States of America 103:18998-19003.
1185 Jadhav AP, Mason HA, Cepko CL. 2006b. Notch 1 inhibits photoreceptor production in
1186 the developing mammalian retina. Development 133:913-923.
1187 James J, Das AV, Rahnenfuhrer J, Ahmad I. 2004. Cellular and molecular
1188 characterization of early and late retinal stem cells/progenitors: Differential regulation of
1189 proliferation and context dependent role of notch signaling. Journal of neurobiology
1190 61:359-376.
1191 Jeon CJ, Strettoi E, Masland RH. 1998. The major cell populations of the mouse retina.
1192 The Journal of neuroscience : the official journal of the Society for Neuroscience
1193 18:8936-8946.
1194 Johnson A, Skotheim JM. 2013. Start and the restriction point. Curr Opin Cell Biol
1195 25:717-723.
1196 Julian LM, Carpenedo RL, Rothberg JL, Stanford WL. 2016. Formula g1: Cell cycle in
1197 the driver's seat of stem cell fate determination. BioEssays : news and reviews in
1198 molecular, cellular and developmental biology 38:325-332.

1199 Jusko TA, Henderson CR, Lanphear BP, Cory-Slechta DA, Parsons PJ, Canfield RL.
1200 2008. Blood lead concentrations < 10 microg/dl and child intelligence at 6 years of age.
1201 Environ Health Perspect 116:243-248.
1202 Kageyama R, Ohtsuka T. 1999. The notch-hes pathway in mammalian neural
1203 development. Cell research 9:179-188.
1204 Kechad A, Jolicoeur C, Tufford A, Mattar P, Chow RW, Harris WA, et al. 2012. Numb is
1205 required for the production of terminal asymmetric cell divisions in the developing
1206 mouse retina. The Journal of neuroscience : the official journal of the Society for
1207 Neuroscience 32:17197-17210.
1208 Koike C, Nishida A, Ueno S, Saito H, Sanuki R, Sato S, et al. 2007. Functional roles of
1209 otx2 transcription factor in postnatal mouse retinal development. Molecular and cellular
1210 biology 27:8318-8329.
1211 Kubo Y, Yasunaga M, Masuhara M, Terai S, Nakamura T, Okita K. 1996. Hepatocyte
1212 proliferation induced in rats by lead nitrate is suppressed by several tumor necrosis
1213 factor alpha inhibitors. Hepatology 23:104-114.
1214 Laughlin NK, Luck ML, Lasky RE. 2009. Early lead exposure effects on an auditory
1215 threshold task in the rhesus monkey (macaca mulatta). Developmental psychobiology
1216 51:289-300.
1217 Leal RB, Ribeiro SJ, Posser T, Cordova FM, Rigon AP, Zaniboni Filho E, et al. 2006.
1218 Modulation of erk1/2 and p38(mapk) by lead in the cerebellum of brazilian catfish
1219 rhamdia quelen. Aquatic toxicology 77:98-104.
1220 Leasure JL, Giddabasappa A, Chaney S, Johnson JE, Jr., Pothakos K, Lau YS, et al.
1221 2008. Low-level human equivalent gestational lead exposure produces sex-specific
1222 motor and coordination abnormalities and late-onset obesity in year-old mice. Environ
1223 Health Perspect 116:355-361.
1224 Leggett RW. 1993. An age-specific kinetic model of lead metabolism in humans.
1225 Environ Health Perspect 101:598-616.
1226 Levine EM, Close J, Fero M, Ostrovsky A, Reh TA. 2000. P27(kip1) regulates cell cycle
1227 withdrawal of late multipotent progenitor cells in the mammalian retina. Developmental
1228 biology 219:299-314.
1229 Levine EM, Green ES. 2004. Cell-intrinsic regulators of proliferation in vertebrate retinal
1230 progenitors. Seminars in cell & developmental biology 15:63-74.
1231 Livesey FJ, Cepko CL. 2001. Vertebrate neural cell-fate determination: Lessons from
1232 the retina. Nature reviews Neuroscience 2:109-118.
1233 Malumbres M, Barbacid M. 2001. To cycle or not to cycle: A critical decision in cancer.
1234 Nature reviews Cancer 1:222-231.
1235 Marquardt T, Gruss P. 2002. Generating neuronal diversity in the retina: One for nearly
1236 all. Trends Neurosci 25:32-38.
1237 Martins RA, Pearson RA. 2008. Control of cell proliferation by neurotransmitters in the
1238 developing vertebrate retina. Brain Res 1192:37-60.
1239 Mendola P, Selevan SG, Gutter S, Rice D. 2002. Environmental factors associated with
1240 a spectrum of neurodevelopmental deficits. Mental retardation and developmental
1241 disabilities research reviews 8:188-197.
1242 Miles A, Tropepe V. 2016. Coordinating progenitor cell cycle exit and differentiation in
1243 the developing vertebrate retina. Neurogenesis 3:e1161697.

1244 Mizeracka K, DeMaso CR, Cepko CL. 2013. Notch1 is required in newly postmitotic
1245 cells to inhibit the rod photoreceptor fate. Development 140:3188-3197.
1246 Murata K, Hattori M, Hirai N, Shinozuka Y, Hirata H, Kageyama R, et al. 2005. Hes1
1247 directly controls cell proliferation through the transcriptional repression of p27kip1.
1248 Molecular and cellular biology 25:4262-4271.
1249 Nagpal AG, Brodie SE. 2009. Supranormal electroretinogram in a 10-year-old girl with
1250 lead toxicity. Documenta ophthalmologica Advances in ophthalmology 118:163-166.
1251 Nelson BR, Hartman BH, Ray CA, Hayashi T, Bermingham-McDonogh O, Reh TA.
1252 2009. Acheate-scute like 1 (ascl1) is required for normal delta-like (dll) gene expression
1253 and notch signaling during retinal development. Developmental dynamics : an official
1254 publication of the American Association of Anatomists 238:2163-2178.
1255 Nowakowski RS, Lewin SB, Miller MW. 1989. Bromodeoxyuridine immunohistochemical
1256 determination of the lengths of the cell cycle and the DNA-synthetic phase for an
1257 anatomically defined population. Journal of neurocytology 18:311-318.
1258 Orrenius S, Zhivotovsky B, Nicotera P. 2003. Regulation of cell death: The calcium-
1259 apoptosis link. Nature reviews Molecular cell biology 4:552-565.
1260 Otto DA, Fox DA. 1993. Auditory and visual dysfunction following lead exposure.
1261 Neurotoxicology 14:191-207.
1262 Pokorski PL, McCabe MJ, Jr., Pounds JG. 1999. Lead inhibits meso-2,3-
1263 dimercaptosuccinic acid induced calcium transients in cultured rhesus monkey kidney
1264 cells. Toxicology 134:19-26.
1265 Ramesh GT, Manna SK, Aggarwal BB, Jadhav AL. 1999. Lead activates nuclear
1266 transcription factor-kappab, activator protein-1, and amino-terminal c-jun kinase in
1267 pheochromocytoma cells. Toxicology and applied pharmacology 155:280-286.
1268 Rapaport DH, Wong LL, Wood ED, Yasumura D, LaVail MM. 2004. Timing and
1269 topography of cell genesis in the rat retina. The Journal of comparative neurology
1270 474:304-324.
1271 Razani-Boroujerdi S, Edwards B, Sopori ML. 1999. Lead stimulates lymphocyte
1272 proliferation through enhanced t cell-b cell interaction. The Journal of pharmacology and
1273 experimental therapeutics 288:714-719.
1274 Rhee KD, Yang XJ. 2010. Function and mechanism of cntf/lif signaling in retinogenesis.
1275 Advances in experimental medicine and biology 664:647-654.
1276 Roegiers F, Jan YN. 2004. Asymmetric cell division. Curr Opin Cell Biol 16:195-205.
1277 Rothenberg SJ, Schnaas L, Salgado-Valladares M, Casanueva E, Geller AM, Hudnell
1278 HK, et al. 2002. Increased erg a- and b-wave amplitudes in 7- to 10-year-old children
1279 resulting from prenatal lead exposure. Investigative ophthalmology & visual science
1280 43:2036-2044.
1281 Rowan S, Conley KW, Le TT, Donner AL, Maas RL, Brown NL. 2008. Notch signaling
1282 regulates growth and differentiation in the mammalian lens. Developmental biology
1283 321:111-122.
1284 Rueda EM, Johnson JE, Jr., Giddabasappa A, Swaroop A, Brooks MJ, Sigel I, et al.
1285 2016. The cellular and compartmental profile of mouse retinal glycolysis, tricarboxylic
1286 acid cycle, oxidative phosphorylation, and ~p transferring kinases. Molecular vision
1287 22:847-885.

1288 Sanchez-Martin FJ, Fan Y, Lindquist DM, Xia Y, Puga A. 2013. Lead induces similar
1289 gene expression changes in brains of gestationally exposed adult mice and in neurons
1290 differentiated from mouse embryonic stem cells. PloS one 8:e80558.
1291 Sasai Y, Kageyama R, Tagawa Y, Shigemoto R, Nakanishi S. 1992. Two mammalian
1292 helix-loop-helix factors structurally related to drosophila hairy and enhancer of split.
1293 Genes & development 6:2620-2634.
1294 Schneider JS, Anderson DW, Wade TV, Smith MG, Leibrandt P, Zuck L, et al. 2005.
1295 Inhibition of progenitor cell proliferation in the dentate gyrus of rats following post-
1296 weaning lead exposure. Neurotoxicology 26:141-145.
1297 Senut MC, Sen A, Cingolani P, Shaik A, Land SJ, Ruden DM. 2014. Lead exposure
1298 disrupts global DNA methylation in human embryonic stem cells and alters their
1299 neuronal differentiation. Toxicological sciences : an official journal of the Society of
1300 Toxicology 139:142-161.
1301 Sherr CJ, Roberts JM. 1999. Cdk inhibitors: Positive and negative regulators of g1-
1302 phase progression. Genes & development 13:1501-1512.
1303 Shimojo H, Ohtsuka T, Kageyama R. 2008. Oscillations in notch signaling regulate
1304 maintenance of neural progenitors. Neuron 58:52-64.
1305 Simons TJ. 1993. Lead-calcium interactions in cellular lead toxicity. Neurotoxicology
1306 14:77-85.
1307 Sobieniecki A, Gutowska I, Machalinska A, Chlubek D, Baranowska-Bosiacka I. 2015.
1308 Retinal degeneration following lead exposure - functional aspects. Postepy higieny i
1309 medycyny doswiadczalnej 69:1251-1258.
1310 Sun Y, Nadal-Vicens M, Misono S, Lin MZ, Zubiaga A, Hua X, et al. 2001. Neurogenin
1311 promotes neurogenesis and inhibits glial differentiation by independent mechanisms.
1312 Cell 104:365-376.
1313 Takahashi T, Nowakowski RS, Caviness VS, Jr. 1993. Cell cycle parameters and
1314 patterns of nuclear movement in the neocortical proliferative zone of the fetal mouse.
1315 The Journal of neuroscience : the official journal of the Society for Neuroscience
1316 13:820-833.
1317 Tomita K, Ishibashi M, Nakahara K, Ang SL, Nakanishi S, Guillemot F, et al. 1996.
1318 Mammalian hairy and enhancer of split homolog 1 regulates differentiation of retinal
1319 neurons and is essential for eye morphogenesis. Neuron 16:723-734.
1320 Vazquez A, Pena de Ortiz S. 2004. Lead (pb(+2)) impairs long-term memory and blocks
1321 learning-induced increases in hippocampal protein kinase c activity. Toxicology and
1322 applied pharmacology 200:27-39.
1323 Verina T, Rohde CA, Guilarte TR. 2007. Environmental lead exposure during early life
1324 alters granule cell neurogenesis and morphology in the hippocampus of young adult
1325 rats. Neuroscience 145:1037-1047.
1326 Vetter ML, Moore KB. 2001. Becoming glial in the neural retina. Developmental
1327 dynamics : an official publication of the American Association of Anatomists 221:146-
1328 153.
1329 Wagner PJ, Park HR, Wang Z, Kirchner R, Wei Y, Su L, et al. 2017. In vitro effects of
1330 lead on gene expression in neural stem cells and associations between up-regulated
1331 genes and cognitive scores in children. Environ Health Perspect 125:721-729.

Wang S, Sengel C, Emerson MM, Cepko CL. 2014. A gene regulatory network controls the binary fate decision of rod and bipolar cells in the vertebrate retina. Developmental cell 30:513-527.
Wu J, Basha MR, Brock B, Cox DP, Cardozo-Pelaez F, McPherson CA, et al. 2008. Alzheimer's disease (ad)-like pathology in aged monkeys after infantile exposure to environmental metal lead (pb): Evidence for a developmental origin and environmental link for ad. The Journal of neuroscience : the official journal of the Society for Neuroscience 28:3-9.
Young RW. 1985a. Cell proliferation during postnatal development of the retina in the mouse. Brain Res 353:229-239.
Young RW. 1985b. Cell differentiation in the retina of the mouse. The Anatomical record 212:199-205.
Zacks DN, Han Y, Zeng Y, Swaroop A. 2006. Activation of signaling pathways and stress-response genes in an experimental model of retinal detachment. Investigative ophthalmology & visual science 47:1691-1695.
Zhang J, Gray J, Wu L, Leone G, Rowan S, Cepko CL, et al. 2004. Rb regulates proliferation and rod photoreceptor development in the mouse retina. Nature genetics 36:351-360.
Zhou ZD, Kumari U, Xiao ZC, Tan EK. 2010. Notch as a molecular switch in neural stem cells. IUBMB life 62:618-623.

Acknowledgements. This work was partially supported by NIH Grants RO1ES012482 to DAF, P30EY07551, T32EY07024 for SYC, and NIOSH-ERC Grant G090168. We thank Margaret Gondo for expert technical assistance and Dr. Connie L. Cepko for valuable discussions.
The authors declare that they have no actual or potential competing financial interests.

Access to Codes:
This work does not contain any codes. Please cite this paper if you use this paper.
Thank you.

FIGURE LEGEND

Supplementary Figure 1, related to Figure 1: Developmental pattern of cell cycle reentry, cell cycle exit and cell fate specification and cell cycle phase lengths in RPCs. GLE induced accelerated cell cycle, increased cell cycle entry, cell cycle exit and cell fate specification. a,b) In mice that were injected with a single pulse of 24 hours before sacrificing for immunohistochemistry analysis of BrdU with MCM6 (a) and OTX2 (b) revealed increased number of MCM6+BrdU+ RPCs reentering cell cycle, increased number of MCM6-BrdU+ RPCs exiting cell cycle, and increased number of BrdU+OTX2+ RPCs becoming postmitotic OTX2+ neurons in GLE. c) In GLE MCM6 and BrdU labeling, 45 min BrdU pulse before sacrificing, reveals accelerated cell cycle or higher proliferation index of RPCs. d) GLE did not alter the G2+M phase of cell cycle calculated as 4.5 hrs from the fraction of $PH3^+$ and $MCM6^+$ colabeled cells counted at 2.5, 3.5 and 4.5 hours following a BrdU injection and the time to reach a mitotic fraction of 1.0 was determined. For all quantifications data are plotted as the mean±sem, *$p<0.05$ and scale bar = 40 µm.

Supplementary Figure 2, related to Figure 3 and Figure 4: Expression of CYCLINs and INKs decreases with developmental age and p27 KIP1 expression peaks at PN4. GLE downregulates expression of INKs and upregulates expression of CYCLINS and p27 KIP1. Immunolabeling of CYCLIN D1(a) and CYCLIN A2(b) are highest in S-phase RPCs in inner retina and also present in RPCs in SVZ of GLE and control retinas. However, in GLE retinas the number of these cyclin colabeled RPCs was increased.

Immunolabeling of cell cycle inhibitors p16 INK4a(c) and p19INK4d(d), and cell cycle exit regulator p27 KIP1(e) are highest in RPCs in SVZ of GLE and control retinas. However, in GLE retinas the number of these cell cycle inhibitor p16INK4a and p19INK4d colabeled RPCs was decreased, while p27 KIP1 cell cycle exit regulator colabeled RPCs was increased. f,g) Quantification by western blot and densitometry show age dependent decreased expression of cell cycle proteins, p107(f) and E2F1(g) consistent with completion of development in control and GLE retinas. In GLE expression of p107 and E2F1 cell cycle proteins were unchanged. All quantifications data are plotted as the mean±sem, *$p<0.05$. Scale bar = 40 µm.

Supplementary Figure 3, related to Figure 5 and Figure 6: Expression of NOTCH1, HES1, OTX2, and MASH1 neuronal cell fate specification factors during development. GLE increases rod and bipolar cell fate specification factors and alters NOTCH1-HES1 pathway. Imunolabeling of OTX2(a) and MASH1(b) are highest in the SVZ RPCs where cell cycle exit and cell fate specification occurs in control and GLE retinas. However, in GLE retinas the number of OTX2 and MASH1 colabeled RPCs was increased. At PN8 OTX2 was localized in inner retina or INBL. c) Immunolabeling of NOTCH1, HES1 and Ki67 shows that early on at PN4 there is more colabeling of RPCs with Hes1 and more labeling of Notch in SVZ in control and GLE retinas consistent with role of NOTCH1-HES1 in maintenance of RPCs. This colabeling of HES1 RPC colabeling was increased in GLE. At PN8 HES1 was localized in inner retina or

INBL (HES1 is known to express in Muller glial cells at this age). For all quantifications data are plotted as the mean±sem, *p<0.05. Scale bar = 40 µm.

Supplement Table 1: Cell Specific Primary Antibodies and Dye Used for Immunohistochemistry (IHC) and Western Blot (WB)

Primary Antigen	Source and Catalog. No.	Target	Host	Dilution	IHC, WB
BrdU	BD Biosciences 347580	Labels RPCs in S phase	Mouse	1:100	IHC
MCM6	Santa Cruz sc-9843	RPCs	Goat	1:100, 1:200	IHC, WB
DRAQ5	Cell signaling technology 4084S	Nucleus		1:250	IHC
CCND1 or Cyclin D1	Santa Cruz sc-450	RPCs	Mouse	1:100, 1:200	IHC, WB
CCNE2 or Cyclin E2	Santa Cruz sc-22777	G1/S phase	Rabbit	1:500	WB
CCNA2 or Cyclin A2	Invitrogen 33-4900	RPCs in S phase	Mouse	1:100, 1:250	IHC, WB
P16Ink4a or CDKN2A	Santa Cruz sc-1661	Early postmitotic cells; few in RPCs	Mouse	1:50, 1:500	IHC, WB
P19Ink4d or CDKN2D	Santa Cruz sc-1063	Perinuclear labeling in early postmitotic cells and few in RPCs	Rabbit	1:50, 1:200	IHC, WB
P27Kip1 or CDKN1B	Cell Signaling Technology 2552	Early postmitotic cells; few in RPCs	Rabbit	1:1000	WB
P27Kip1 or CDKN1B	BD Biosciences 610241	Early postmitotic cells; few in RPCs.; also Muller cells.	Mouse	1:100	IHC
CDK4	Santa Cruz sc-260	G1 phase cyclin dependent kinase	Rabbit	1:50	WB
CDK2	Santa Cruz sc-6248	S and G2 phase cyclin dependent kinase	Mouse	1:50	WB
p-CDK2 (Thr 160)	Santa Cruz sc-101656	Activated Cdk2	Rabbit	1:50	WB
RB1	BD Biosciences 554136	Retinoblastoma protein	Mouse	1:250	WB
p-RB1 (Ser 780)	Cell Signaling Technology 9307S	Hyperphosphorylated-RB	Rabbit	1:1000	WB
P107	Santa Cruz sc-318	P107 from RB family	Rabbit	1:200	WB
E2F1	Santa Cruz sc-193X	E2F1 transcription factor	Rabbit	1:1000	ChIP-PCR
C-JUN	Santa Cruz sc-45X	C-JUN transcription factor	Rabbit	1:1000	ChIP
POL II (N-20)	Santa Cruz sc-899	RNA Polymerase	Rabbit	1:1000	ChIP
PH3 (Ser10)	Upstate 06-570	Labels RPCs in M phase	Rabbit	1:40	IHC
Otx2	Chemicon AB9566	OTX2 homeodomain protein	Rabbit	1:100 1:200	IHC WB
Ki67	BD 550609	Retinal progenitor cells	Mouse	1:100	IHC
MASH1	Chemicon ab15582	RPC, and Differentiating neurons	Rabbit	1:100 1:1000	IHC WB
HES6	Gift	bHLH transcription factor HES6	Rabbit	1:100	WB
NEUROD1	Chemicon AB5686	bHLH transcription factor NEUROD1	Rabbit	1:500	WB
STAT3	Cell Signaling 9139	STAT3 transcription factor	Mouse	1:500	WB
pSTAT3 (Tyr705)	Cell Signaling 9145	Activated STAT3	Rabbit	1:500	WB
NOTCH1	Santa Cruz sc-6015	NOTCH1 membrane protein	Goat	1:100	IHC
NOTCH1-ECD	Upstate 07-218	NOTCH1 membrane protein	Rabbit	1:1000	WB
NOTCH1-ICD	Upstate 07-220	Internal cleaved active NOTCH1	Rabbit	1:1000	WB
HES1	Chemicon ab5702	RPCs, and Muller glial cells	Rabbit	1:100 1:1000	IHC WB

Supplement Table 2: RT-qPCR and ChIP-PCR Gene-Specific Forward and Reverse primers

Gene	Forward Primer (5'–3')	Reverse Primer (5'–3')	Product Size (bp)	Location intron
Cyclin D1-1	aacaagcagaccatccgcaa	tggagggtgggttggaaatgaa	85	Exons 3–4
Ccne2	gccatcgactctttagaatttca	tgtcatcccattccaaacct	109	769(1157)
Ccna2-2	gtcaaccccgaaaaactgg	aaggtccttaagaggagcaacc	129	655(360)
p19-1	gtcggcgaccggttgagt	tgctggacttccaaacatca	144	401
P16	cgacgggcatagcttcag	gctctgctcttgggattgg		
P27-1	agtgtccagggatgaggaag	tctgttctgttggccctttt	73	559 bp
Mcm6-1	acctgtaccacaatctctgcac	caccgcgttttacttcatca	69	2353(1169)
Cdk4	tcagtggtgccagagatgg	ggaaggcagagattcgctta	88	992
Cdk2	ctgcatctttgctgaaatgg	gatccggaagagttggtcaat		
Rb1-1	aaagaagtgctgaaggcggcaa	aatttggactccgctgggagat	112	Exons 24–25
P107-1	gcggcaactacagcctaga	tgcggcaagcaacatataaa	69	4747
E2f1-1	tgccaagaagtccaagaatca	cttcaagccgcttaccaatc	74	804
Rb1-pro2	caacccgcaaaagtggaa	atccggcctcctttcataat	78	-597/-674;chr14: 73726195-73726272
CCND1-pro3	ctagctgtcctcctgtccaga	gggcttctttccctaagagg	77	(upstream)_248 to _172
Otx2	ggtatggacttgctgcatcc	cgagctgtgccctagtaaatg	91	992
Neurod1	gcagaaggcaaggtgtcc	tttggtcatgtttccacttcc	89	1497
Ascl1	cgaatcacagatgggttcct	gtggttgggagttaatatagtgtctg	88	20494
Hes6	acggatcaacgagagtcttca	ttctctagcttggcctgcac	72	84
Notch1	ctggaccccatggacatc	aggatgactgcacacattgc	73	1012
Hes1	acaccggacaaaccaaagac	cgcctcttctccatgatagg	68	130
Stat3	tggcaccttggattgagag	caacgtggcatgtgactctt	65	2427
Ascl1	tgtttattcagccgggagtc	gctccttgcaaactctcca	84	-183/-266;chr10: 86956588-86956671
ß-actin	agagaggtatcctgaccctgaagt	cacgcagctcattgtagaaggtgt	105	262-366

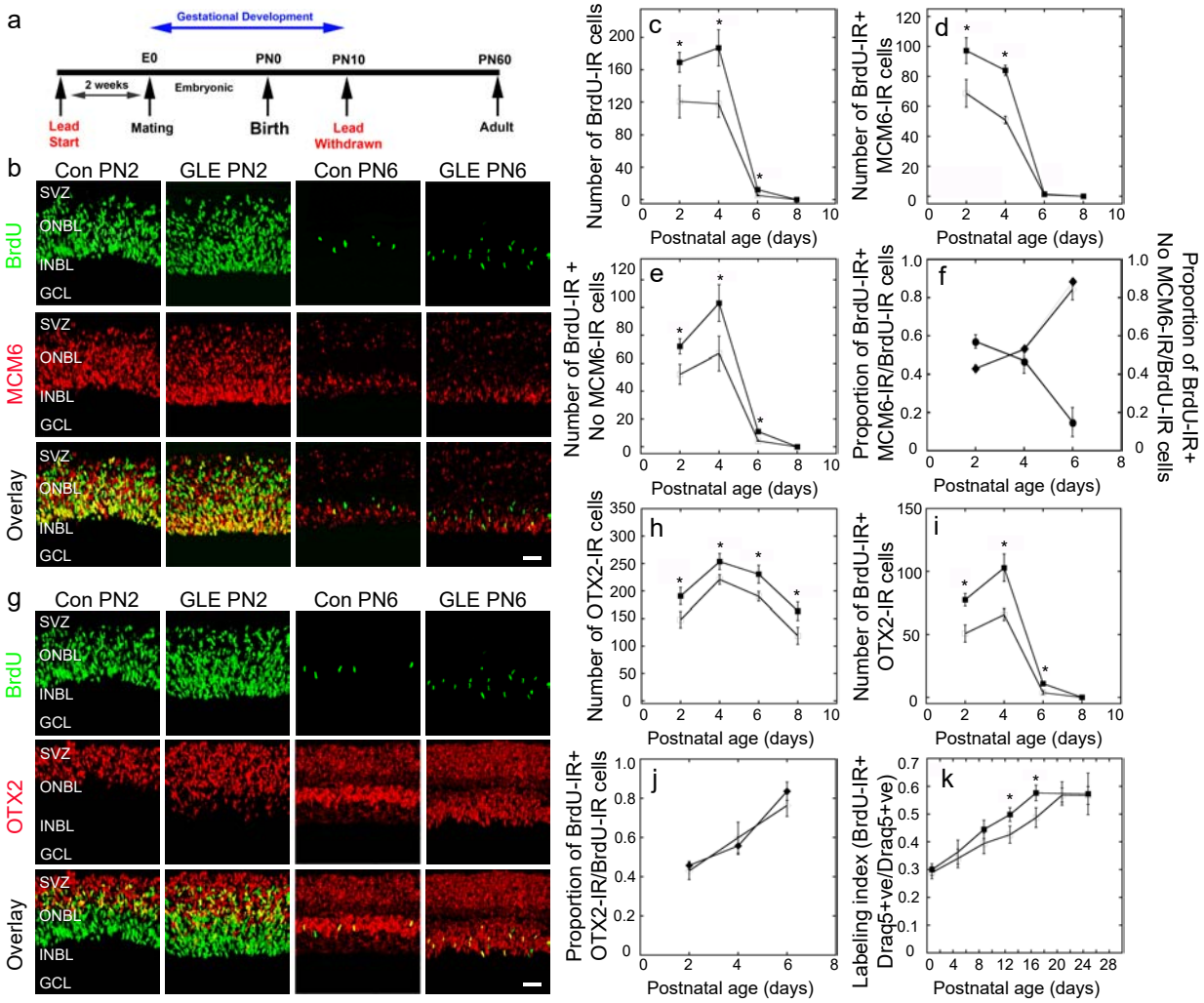

Figure 1 Mukherjee

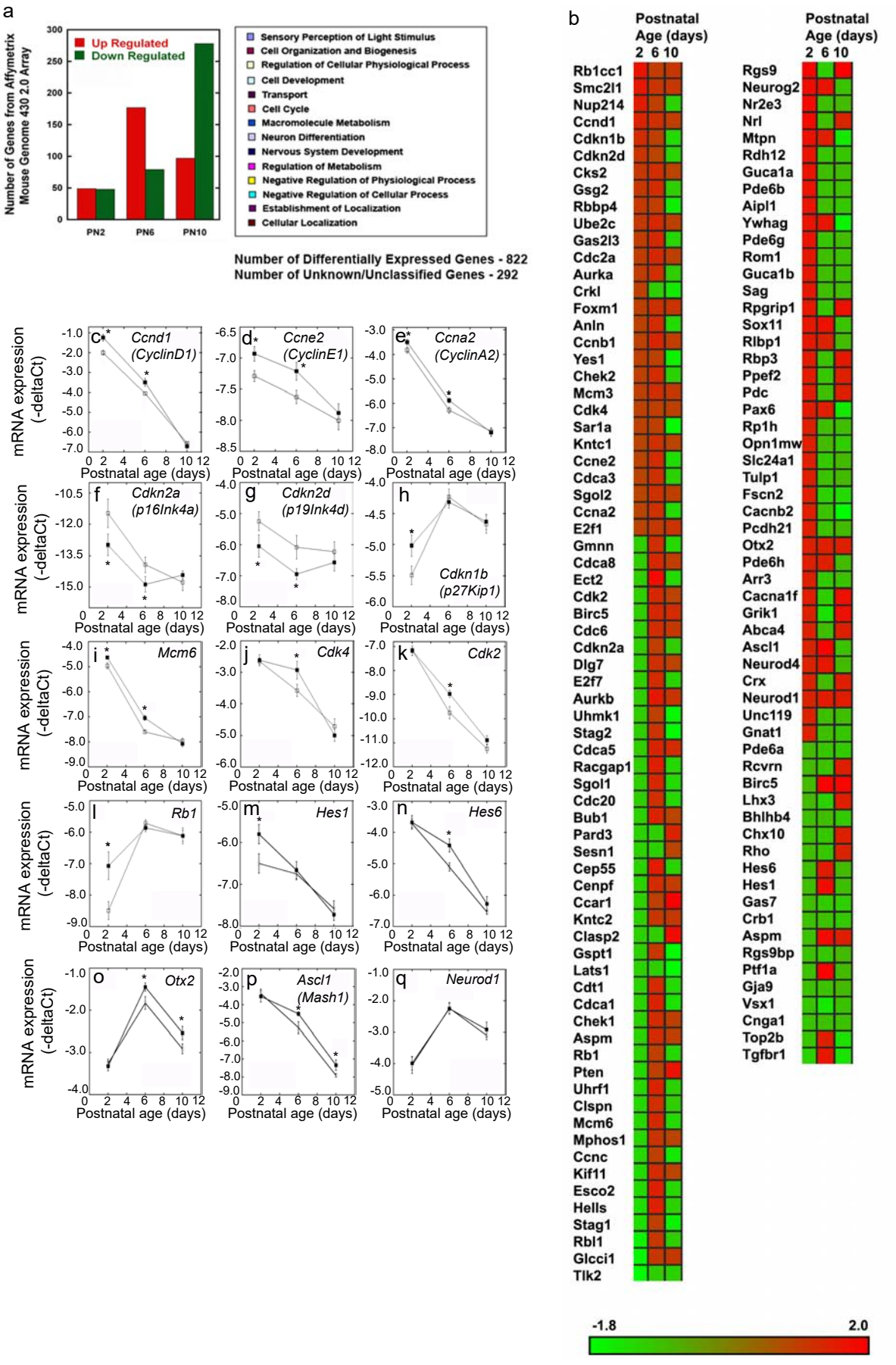

Figure 2 Mukherjee

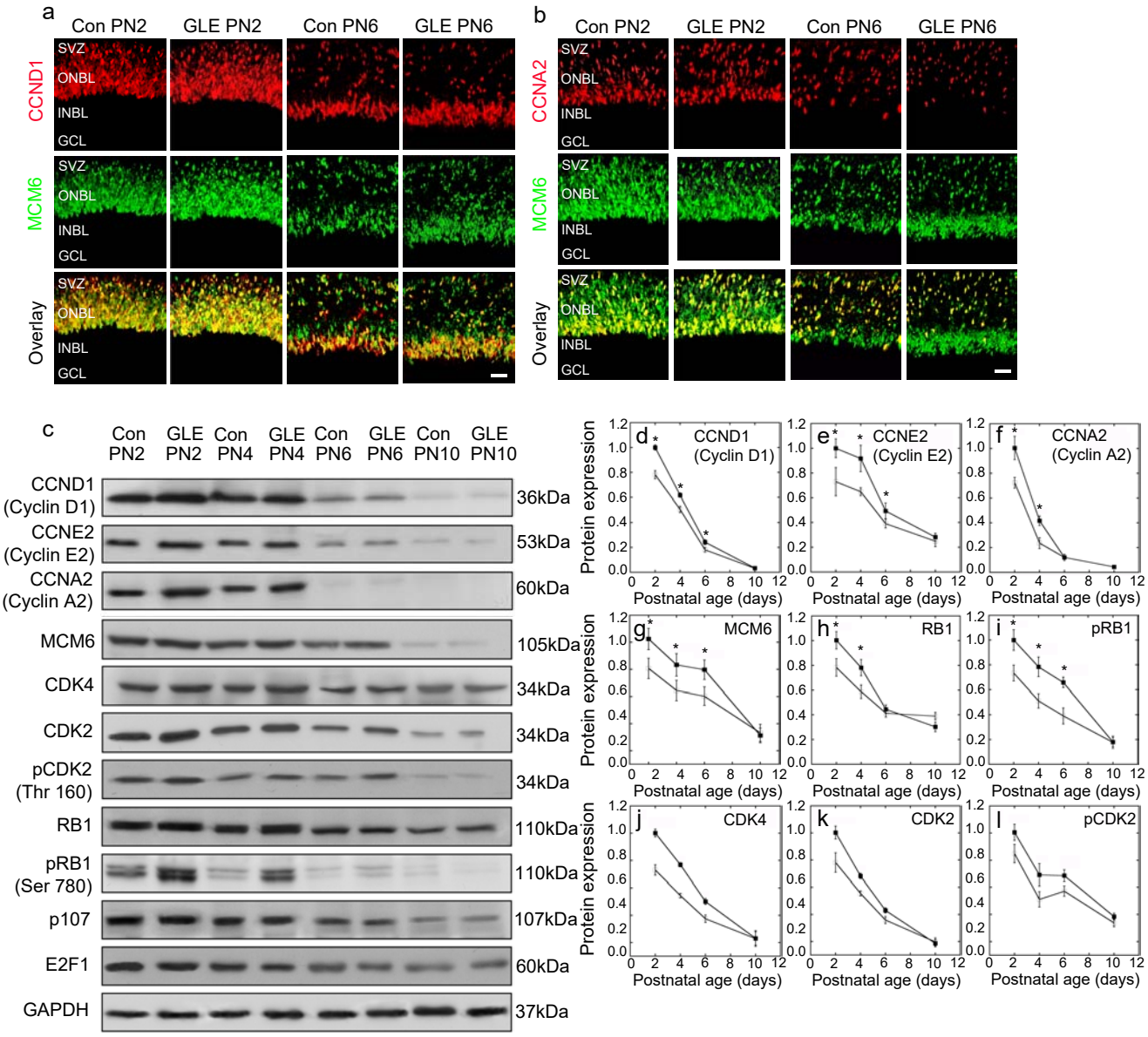

Figure 3 Mukherjee

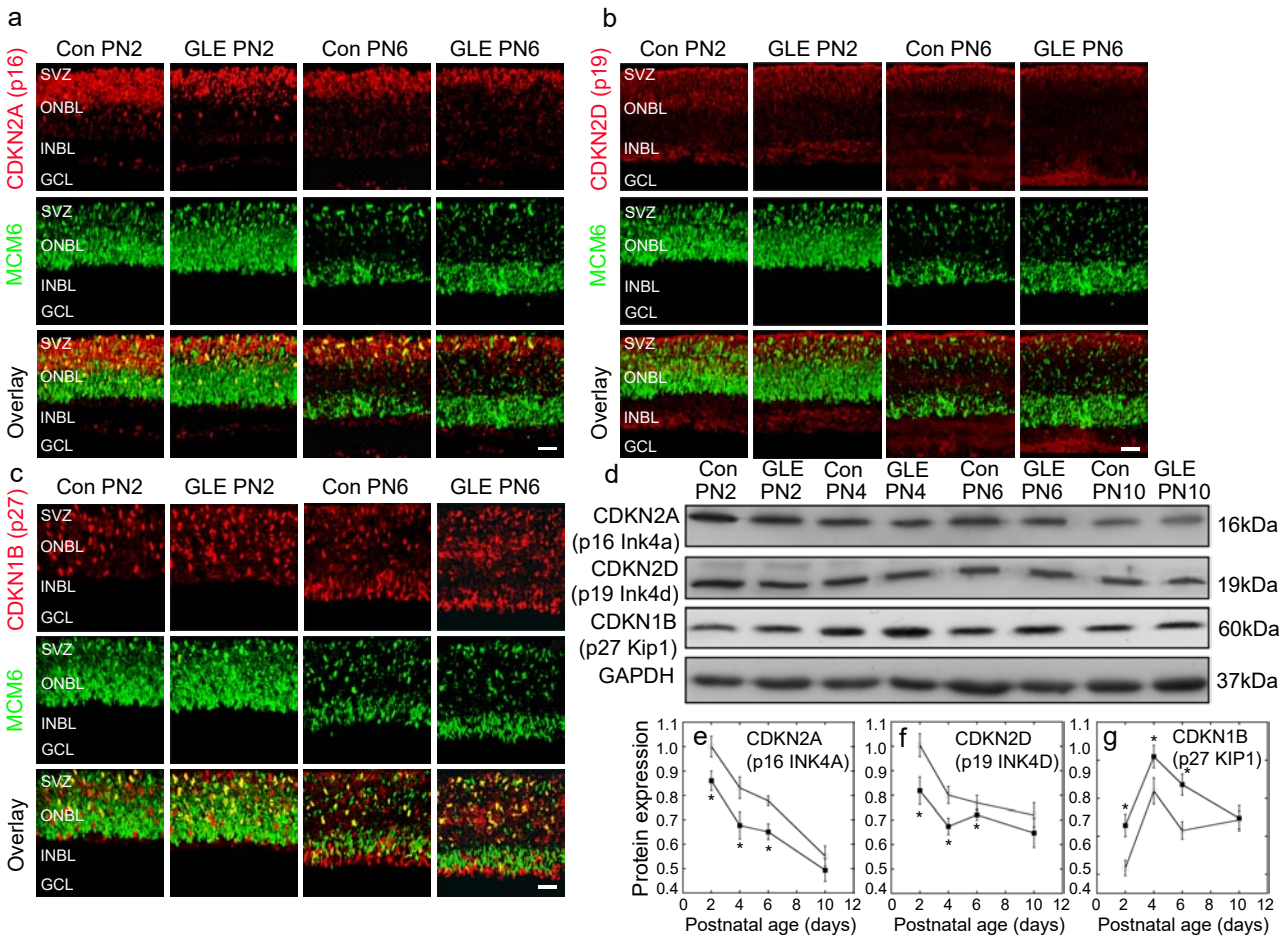

Figure 4 Mukherjee

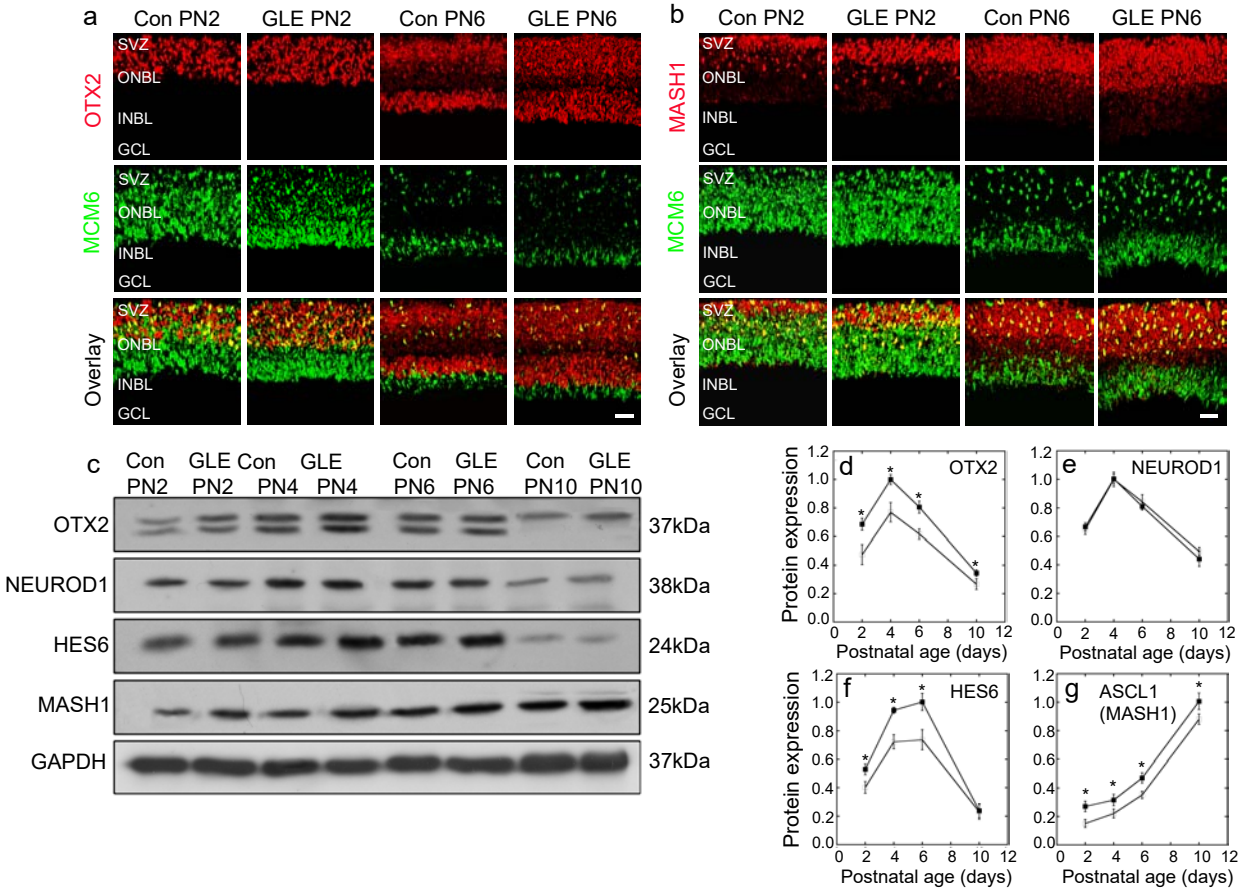

Figure 5 Mukherjee

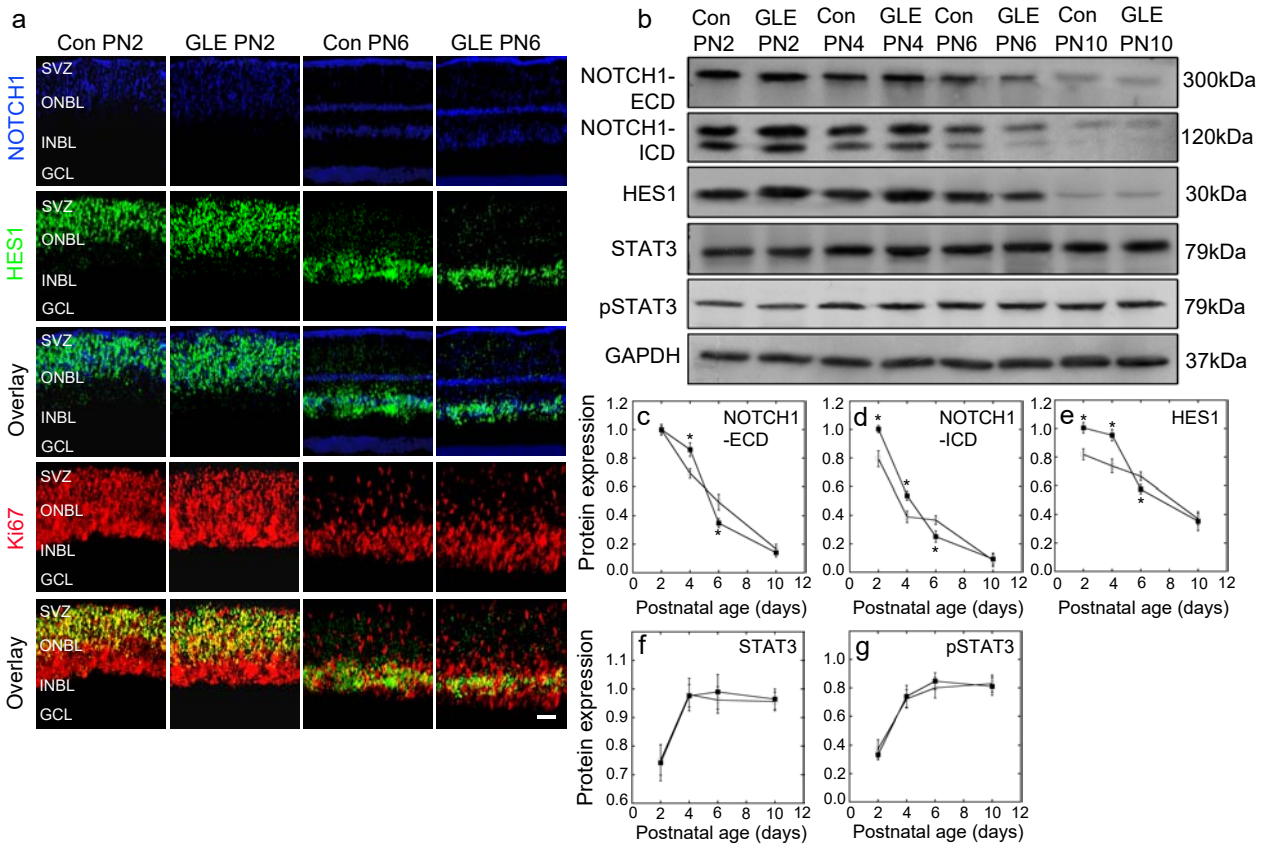

Figure 6 Mukherjee

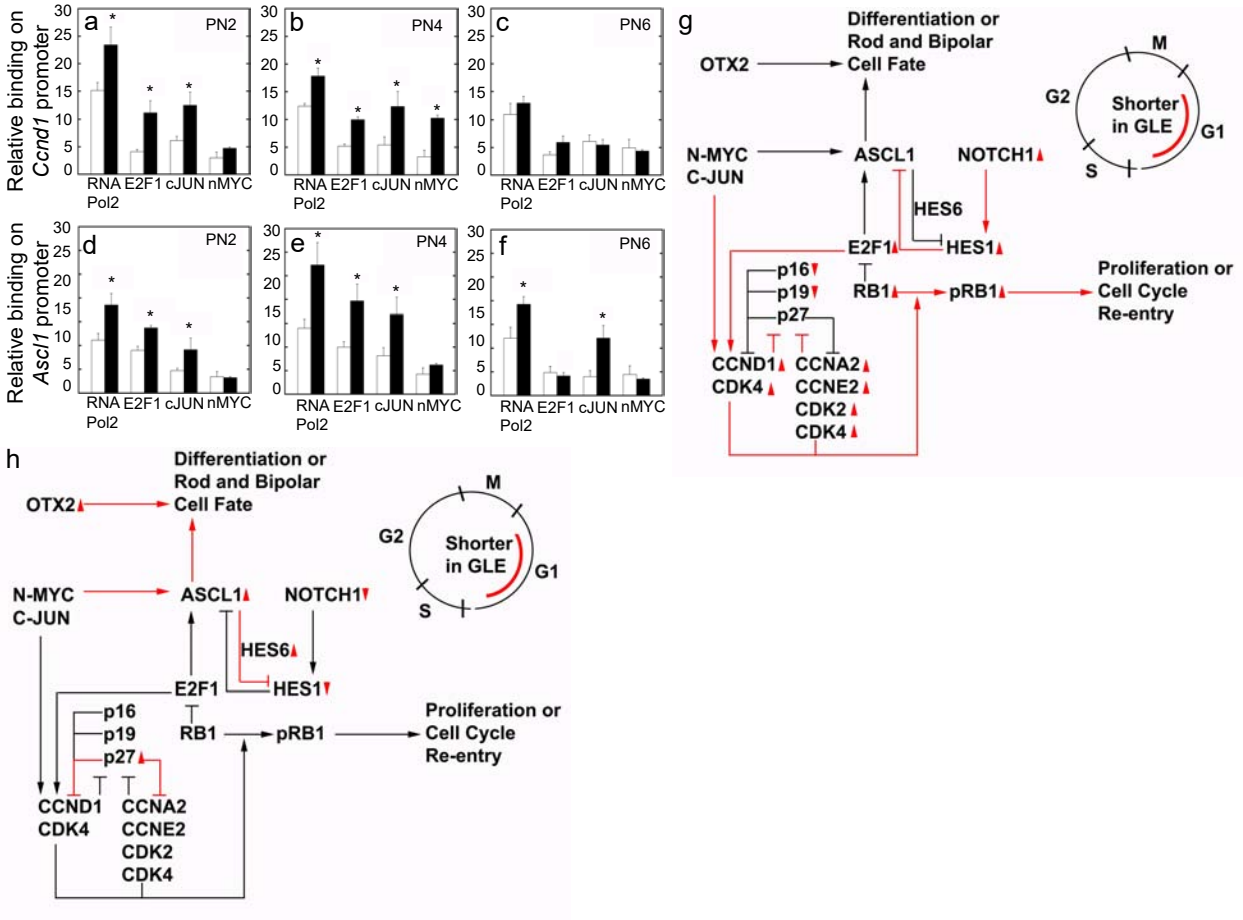

Figure 7 Mukherjee

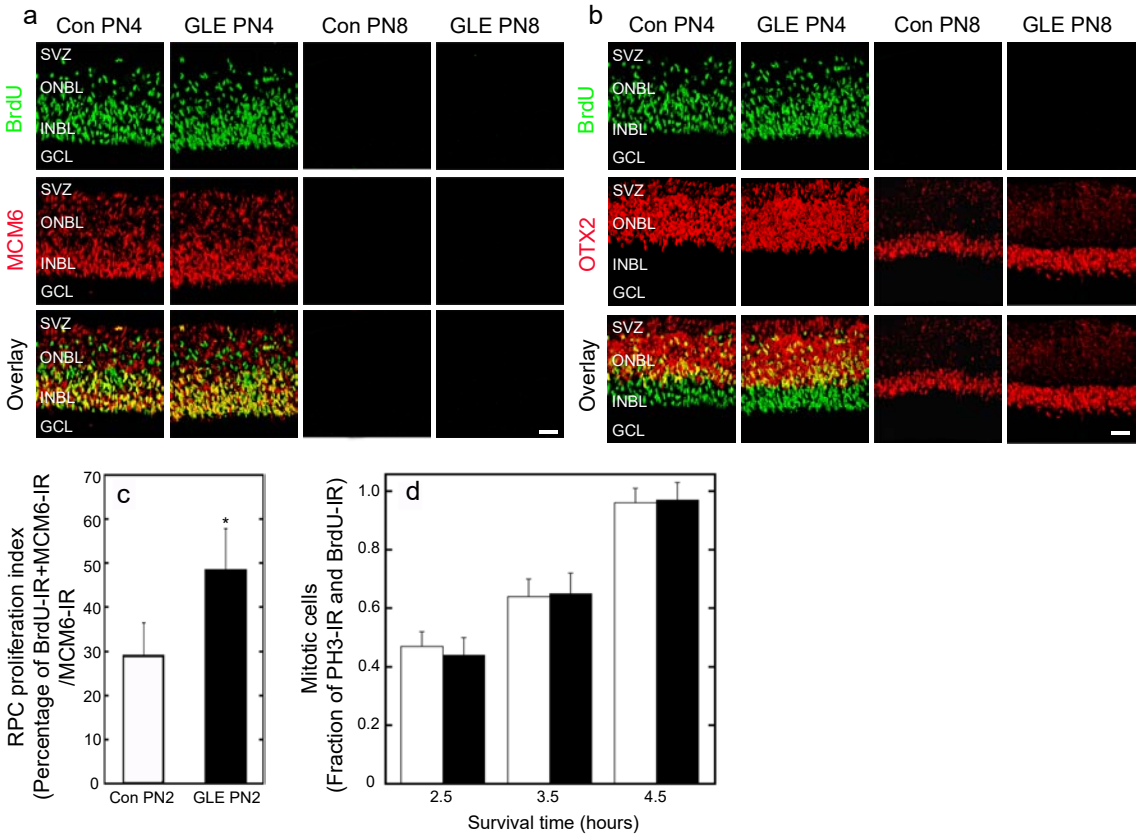

Supplementary Figure 1 Mukherjee

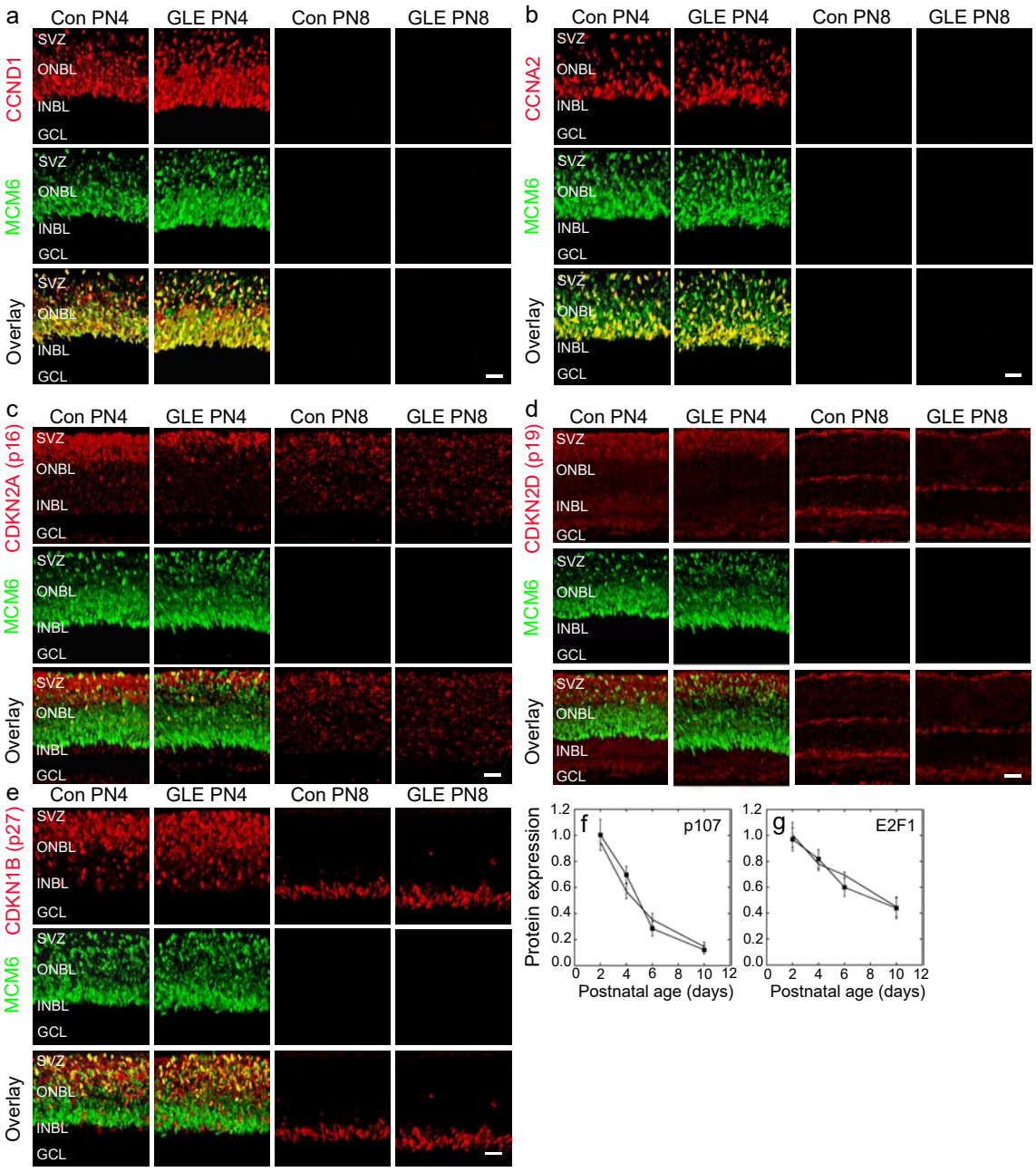

Supplementary Figure 2 Mukherjee

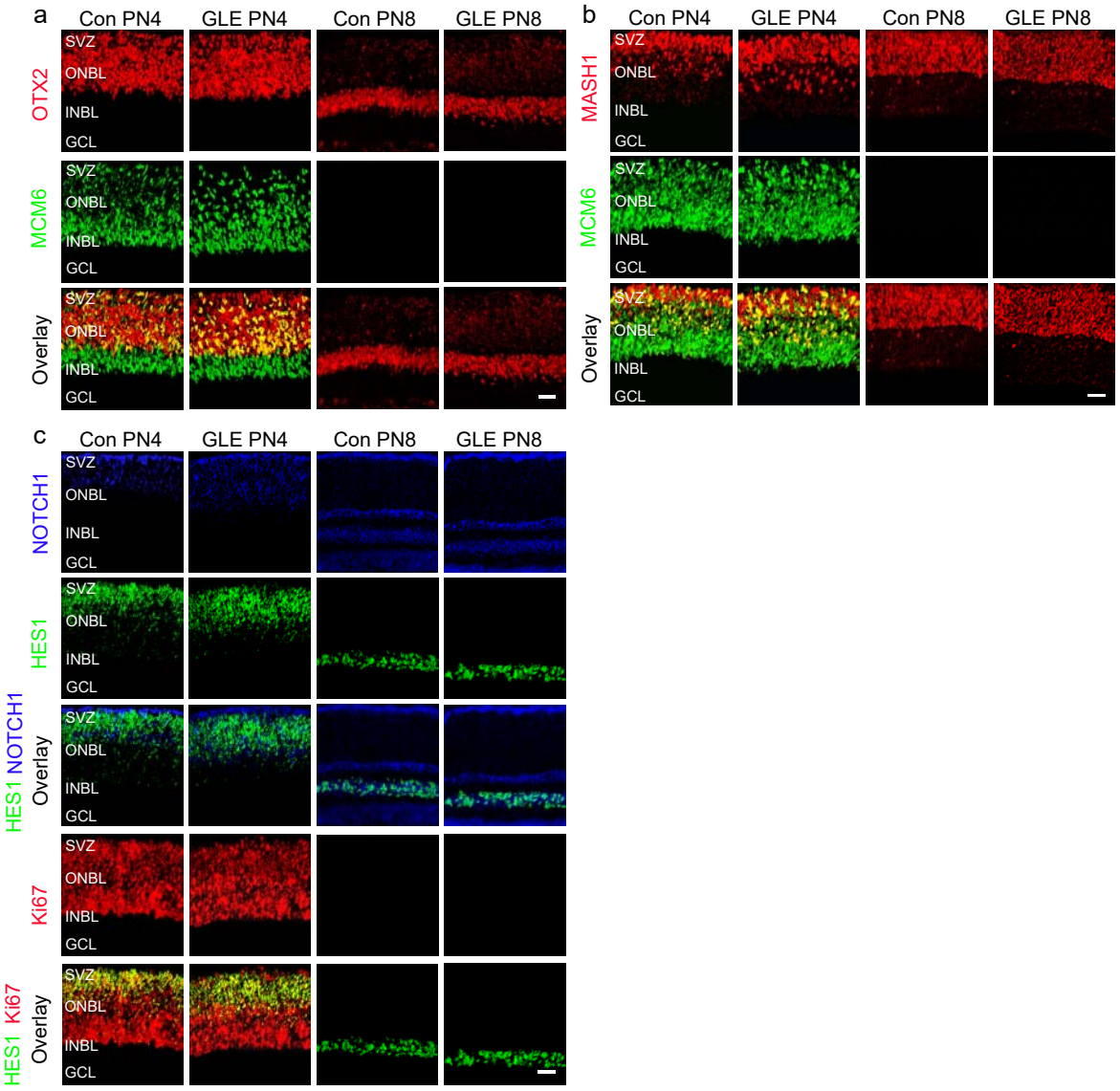

Supplementary Figure 3 Mukherjee